Journal of Rock Mechanics and Geotechnical Engineering 16 (2024) 1467–1485

Contents lists available at ScienceDirect

Journal of Rock Mechanics and Geotechnical Engineering

journal homepage: www.jrmge.cn

Review

A review of in situ carbon mineralization in basalt

Xiaomin Cao [a,b], Qi Li [a,b,*], Liang Xu [a,b], Yongsheng Tan [a,b]

[a] State Key Laboratory of Geomechanics and Geotechnical Engineering, Institute of Rock and Soil Mechanics, Chinese Academy of Sciences, Wuhan 430071, China
[b] University of Chinese Academy of Sciences, Beijing 100049, China

ARTICLE INFO

Article history:
Received 9 August 2023
Received in revised form
21 October 2023
Accepted 20 November 2023
Available online 25 December 2023

Keywords:
Carbon mineralization
Basalt
CO_2-fluid-basalt interaction
Petrophysical evolution
Mechanical response
Carbon capture and storage (CCS)

ABSTRACT

Global warming has greatly threatened the human living environment and carbon capture and storage (CCS) technology is recognized as a promising way to reduce carbon emissions. Mineral storage is considered a reliable option for long-term carbon storage. Basalt rich in alkaline earth elements facilitates rapid and permanent CO_2 fixation as carbonates. However, the complex CO_2-fluid-basalt interaction poses challenges for assessing carbon storage potential. Under different reaction conditions, the carbonation products and carbonation rates vary. Carbon mineralization reactions also induce petrophysical and mechanical responses, which have potential risks for the long-term injectivity and the carbon storage safety in basalt reservoirs. In this paper, recent advances in carbon mineralization storage in basalt based on laboratory research are comprehensively reviewed. The assessment methods for carbon storage potential are introduced and the carbon trapping mechanisms are investigated with the identification of the controlling factors. Changes in pore structure, permeability and mechanical properties in both static reactions and reactive percolation experiments are also discussed. This study could provide insight into challenges as well as perspectives for future research.

1. Introduction

The burning of massive amounts of fossil fuels since the Industrial Revolution has led to a surge in greenhouse gas emissions. According to the Intergovernmental Panel on Climate Change (IPCC) Special Report on Global Warming of 1.5 °C, anthropogenic activities have resulted in a global temperature increase of 0.8–1.2 °C compared to preindustrial levels (IPCC, 2022). Global warming is roughly proportional to the total amount of CO_2 released into the atmosphere, and it is imperative to reduce the CO_2 level in the atmosphere. Carbon capture and storage (CCS) technology is recognized as an effective way to address the current climate problem (Xu et al., 2019).

The CCS technology refers to capturing and separating CO_2 from large carbon emission sources or directly capturing CO_2 from the atmosphere and then injecting it into saline aquifers, oil and gas fields, deep coal seams or the deep ocean regions to achieve permanent storage of CO_2 (Li et al., 2022b). The storage of CO_2 mainly involves four mechanisms: (1) Structural trapping. CO_2 is blocked from moving upward due to the sealing effect of low permeability caprock, thus being sealed under the caprock (Iglauer, 2018). (2) Solution trapping. CO_2 dissolves in formation water as an aqueous phase. (3) Residual trapping. In the process of water re-imbibition, the CO_2 plume is subjected to capillary forces and dispersed into discontinuous immobile blobs (Bonto et al., 2021). (4) Mineral trapping. CO_2 reacts with host rocks to form stable carbonate minerals. At the initial stage of the CCS project, the dominant mechanism is structural trapping. Over longer time scales, CO_2 will either dissolve into the formation water or become fixed as carbonate minerals. However, since CO_2 has a lower density than water or crude oil, it floats upward and may escape along the weakest zone of caprock or wells (Song et al., 2023). There is a potential risk of leakage during long-term geological storage, and thus, mineral trapping is the most secure and reliable form of permanent CO_2 storage. Traditional sandstone reservoirs are typically unreactive, requiring tens of thousands of years to undergo complete mineralization.

Several natural phenomena have shed new light on carbon mineralization in basalt. For example, in the central basin of the South China Sea, there are abundant carbonate veins occurring at the top and bottom of lava flows, which are mostly the carbonation

* Corresponding author. State Key Laboratory of Geomechanics and Geotechnical Engineering, Institute of Rock and Soil Mechanics, Chinese Academy of Sciences, Wuhan 430071, China.
E-mail address: qli@whrsm.ac.cn (Q. Li).

Peer review under responsibility of Institute of Rock and Soil Mechanics, Chinese Academy of Sciences.

https://doi.org/10.1016/j.jrmge.2023.11.010

products of olivine and plagioclase (Li et al., 2022a). In addition, the brecciated-veined textures pervasively exist in the Malentrata area with Fe-rich magnesite cores and Fe-poor dolomite borders, which are the carbonation products of serpentine alteration (Boschi et al., 2009). The presence of these natural silicate alteration products confirms the feasibility of basalt mineralization. In fact, mafic basalt is the most widely distributed igneous rock, constituting about 70% of the oceanic floor and >5% of the land area, as shown in Fig. 1 (Snaebjornsdottir et al., 2020). Basalt contains many Ca-, Mg- and Fe-bearing silicate minerals and is rich in alkaline earth elements, which can quickly form stable carbonate minerals with the injected CO_2 (Raza et al., 2022; Seifritz, 1990). Global natural basalt weathering can consume 180 million tons of CO_2 every year, accounting for approximately one-third of CO_2 absorbed by rocks in the atmosphere (Matter and Kelemen, 2009). Although this is of great significance for regulating global climate change and the carbon cycle, it is still far from meeting the demand for human carbon emission reduction. It is necessary to artificially inject CO_2 into the basalt reservoirs and accelerate in situ carbon mineralization process by certain technical means to implement a considerable number of storage tasks. Currently, in situ carbon mineralization technology in basalt is in the stage of pilot demonstration worldwide. The CarbFix pilot in Iceland and the Wallula pilot in the United States successfully injected 248 t and 1000 t of CO_2 into basalt formations and achieved 95% (Matter et al., 2016) and 60% (White et al., 2020) mineralization within two years, respectively. These two pilots greatly encouraged the determination to implement in situ carbon mineralization storage in basalt and promoted the progress of this technology.

Carbon mineralization process can be divided into three steps, including CO_2 dissolution and dissociation, silicate dissolution and carbonate precipitation. The dissolution and dissociation of CO_2 is a function of temperature, pressure and salinity (Mohammadian et al., 2023), while the dissolution and precipitation processes of basalt are controlled by several factors. The major influencing factors include the mineral compositions and pore structure of the host rock, temperature, pH, CO_2 pressure, injection rate and the chemical compositions of both the formation water and the injected fluid, etc. Under different reaction conditions, the carbonation products and rates vary (Gadikota et al., 2020; Kumar and Shrivastava, 2019). Along with mineral dissolution or precipitation, the pore structure, permeability and mechanical properties of reservoir also change. In general, the dissolution of minerals might propagate the preexisting cracks and defects, and lead to the generation of new pores and etch pits, which would impair the mechanical strength concurrently (Guha Roy et al., 2016). The localized precipitations might obstruct the transport channels and reduce the permeability of reservoir, thus affecting the long-term injectivity (Peuble et al., 2015b).

Before large-scale industrial application, several key problems need to be addressed: (1) What about the carbon storage potential and mineralization rate? (2) What are the major influencing factors and mechanisms that affect the carbon mineralization reaction? (3) What conditions are more favorable for carbon storage in basalt? (4) How do the petrophysical and mechanical properties change due to CO_2-basalt-fluid interaction? (5) How to overcome or reduce the adverse effect induced by carbon mineralization reaction? Laboratory experiments provide a fundamental means to address these questions. However, there is currently a lack of a systematic summary of the influencing factors on basalt carbonation mechanisms and the existing reviews mainly focus on the implementation of carbon mineralization in basalt (Matter and Kelemen, 2009; Oelkers et al., 2008; Snaebjornsdottir et al., 2020).

This study aims to provide a comprehensive understanding of the mechanisms of CO_2-basalt-fluid interaction and the induced petrophysical and mechanical responses based on laboratory experiments. In Section 2, the methods of carbon storage potential assessment, carbon mineralization process and experimental

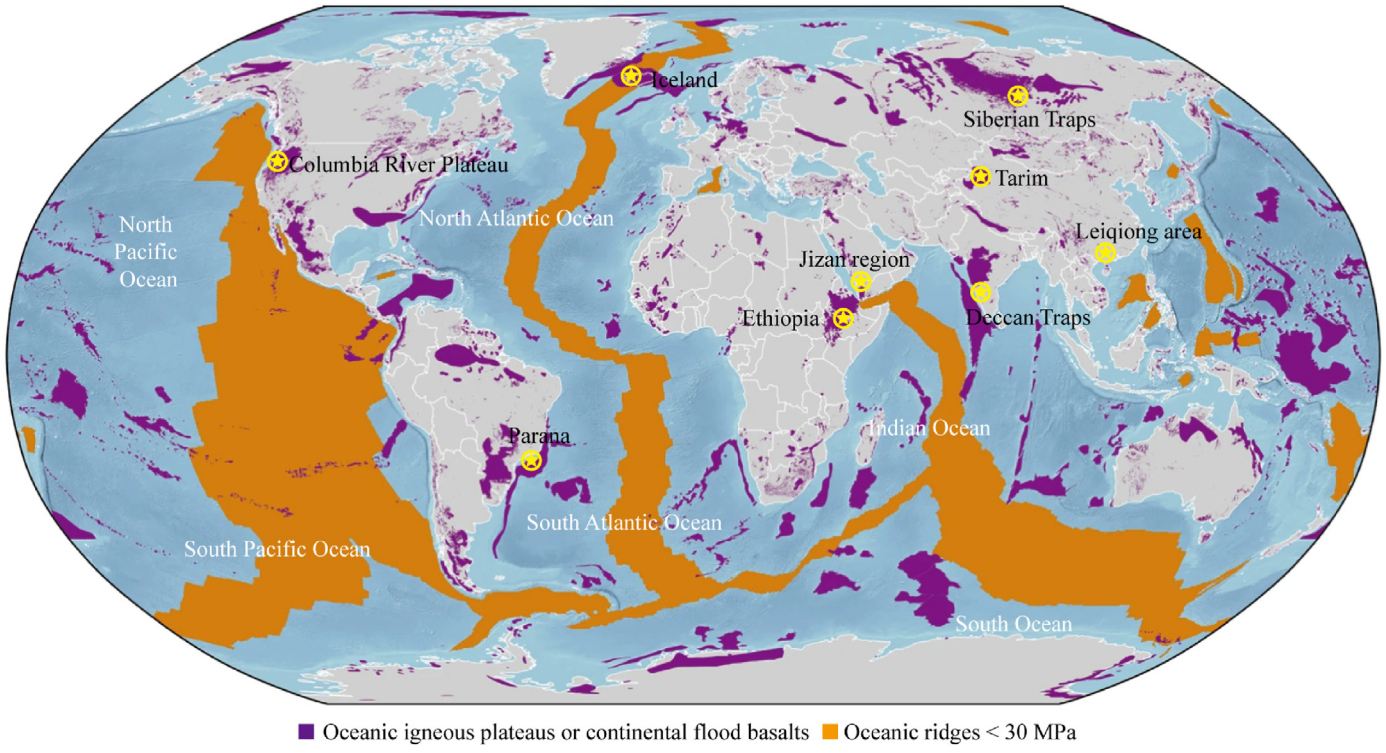

Fig. 1. Locations of mafic basalts for in situ carbon mineralization (Snaebjornsdottir et al., 2020).

Table 1
Potential basalt formations for in situ carbon mineralization and preliminary carbon storage capacity estimations.

Location	Type	Porosity (%)	Area (km^2)	Volume (km^3)	Capacity (Gt)	Evaluation methods	References
Offshore Iceland (Iceland)	MORB	10	93,000	93,000	2600–6800	Natural analogy method	Snæbjörnsdóttir and Gislason (2016)
India	CFB	10–15	500,000	512,000	97–316	Natural analogy method	Vishal et al. (2021)
Jizan region (Saudi Arabia)	CFB	–	150	150	1.4–10.2	Natural analogy method	Oelkers et al. (2022)
Juan de Fuca Ridge (USA)	MORB	10	78,000	7800	900	Pore-filling method	Goldberg et al. (2008)
Onshore Iceland (Iceland)	MORB	10	103,000	10,300	1210	Pore-filling method	Anthonsen et al. (2013)
Leizhou Peninsula (China)	OIB	8.9	3940	257	30.8–45.9	Complete mineralization method	Li et al. (2023)
China	–	–	593,831–594,541	–	201.1–1121.4	Complete mineralization method	Zhang et al. (2023)

methodology are elaborated. In Section 3, the carbon trapping mechanism is investigated from silicate dissolution and carbonate precipitation processes. Additionally, the passivation effect generated by secondary mineral coating is also stated. In Section 4, the evolution of petrophysical and mechanical properties induced by CO_2-basalt-fluid interaction is discussed. In Section 5, the details of two successful field pilot projects, CarbFix and Wallula, are provided. The conclusion, challenges and future perspectives are then proposed.

2. Carbon mineralization reaction

2.1. Carbon storage potential assessment

Basalt is the most widely distributed igneous rock on Earth, with SiO_2 content between 45% and 53%. It is rich in Ca-, Mg-, and Fe-bearing minerals, such as olivine ($(Mg,Fe)_2SiO_4$), pyroxene ($(Mg,Fe,Ca)_2Si_2O_6$) and plagioclase (albite ($NaAlSi_3O_8$) to anorthite ($CaAl_2Si_2O_8$)), as well as their amorphous equivalents. Empirical evidence suggests that continental flood basalt (CFB), Mid-ocean ridge basalt (MORB) and ocean-island basalt (OIB) possess substantial carbon storage potential (Li et al., 2022c).

Theoretical CO_2 storage capacity serves as a crucial criterion for the selection of basalt reservoirs. McGrail et al. (2006) first estimated that Columbia River Basalt (CRB) could sequester 100 Gt of CO_2 using a method akin to saline aquifer storage, where CO_2 exists in a supercritical form in pore space. However, given the high reactivity of basalt, most of the injected CO_2 will be sequestered as carbonates rather than remaining in a supercritical or aqueous phase. Based on basalt carbonation reactions, there are three commonly used methods for evaluating the carbon storage potential of basalt (Amy et al., 2012; Goldberg et al., 2008; Snæbjörnsdóttir and Gislason, 2016).

The first approach is the natural analogy method, which utilizes field or experimental data to obtain the carbon storage capacity per unit volume of basalt and then extrapolates it to estimate the carbon storage potential of the entire site. This procedure considers the reactivity of basalt in different locations and is relatively accurate and representative. Applying the amount of CO_2 fixed in geothermal systems in Iceland (Snæbjörnsdóttir et al., 2014), with a minimum of 18.8 kg/m^3 and a maximum of 48.7 kg/m^3, respectively, offshore Iceland has the potential to sequester 2600–6800 Gt CO_2 (Snæbjörnsdóttir and Gislason, 2016). The second methodology is the pore-filling method, which assumes all pore spaces are filled with carbonate precipitates to estimate the carbon storage capacity (Goldberg et al., 2008), and is more effective for reservoirs with lower porosity. Assuming that all of the injected CO_2 is fixed as $CaCO_3$, Juan de Fuca Ridge could potentially hold 900 Gt CO_2 (Goldberg et al., 2008). The third method is the complete mineralization method, which presumes that all CaO, MgO and FeO in the basalt will react fully with CO_2 to form Ca–Mg–Fe carbonates (Amy et al., 2012). On this basis, the carbon storage capacity of Leizhou Peninsula was estimated to be 30.8–45.9 Gt (Li et al., 2023). However, in reality, Ca, Mg and Fe are unlikely to be completely fixed in carbonate minerals, so this method provides an estimate of the maximum mineralization capacity of the reservoir. An improved complete mineralization method is thus put forward. Zhang et al. (2023) introduced an effective storage coefficient that takes into account the swept area of injected CO_2 and reaction degree of silicate minerals, and estimated the effective carbon storage potential of terrestrial basalts in China reached 201.1–1121.4 Gt. Table 1 summarizes the carbon storage capacity of some basalt formations based on the abovementioned methods, but importantly, the estimations are preliminary.

2.2. In situ carbon mineralization process

The carbon mineralization process in basalt mainly includes CO_2 dissolution and dissociation, proton consumption and divalent cation release during the dissolution of silicate minerals and carbonate minerals precipitation, as shown in Fig. 2.

(1) Carbonic acid formation: The injected CO_2 dissolves in formation water and dissociates into H^+, HCO_3^- and CO_3^{2-} ions. The pH of the formation water subsequently decreases, and the extent of the pH decline mainly depends on the temperature, CO_2 pressure and salinity of the formation water. The hydration reactions of CO_2 are as follows:

$$CO_2(aq) + H_2O \rightleftarrows H_2CO_3 \rightleftarrows H^+ + HCO_3^- \rightleftarrows H^+ + CO_3^{2-} \quad (1)$$

(2) Silicate dissolution: During the dissolution process, many divalent cations (Ca^{2+}, Mg^{2+} and Fe^{2+}) are released for CO_2 fixation, and H^+ ions are consumed, resulting in an increased pH (Eq. (2)), which is conducive to carbonate mineral precipitation.

$$2H^+ + (Ca, Mg, Fe)SiO_3 \rightleftarrows Ca^{2+}, Mg^{2+}, Fe^{2+} + SiO_2(aq) + H_2O \quad (2)$$

The progress of silicate dissolution can be divided into three steps (Oelkers, 2001; Oelkers and Gislason, 2001). First, the monovalent and divalent cations quickly enter the solution via exchange adsorption. Then, the Al–O bonds are destroyed by the Al-proton exchange reaction, and Al atoms are removed. Finally, the partially detached Si–O structure slowly liberates and hydrolyzes. Silicate minerals containing no Al atoms exhibit a higher dissolution rate because the partially detached Si–O bonds are destroyed

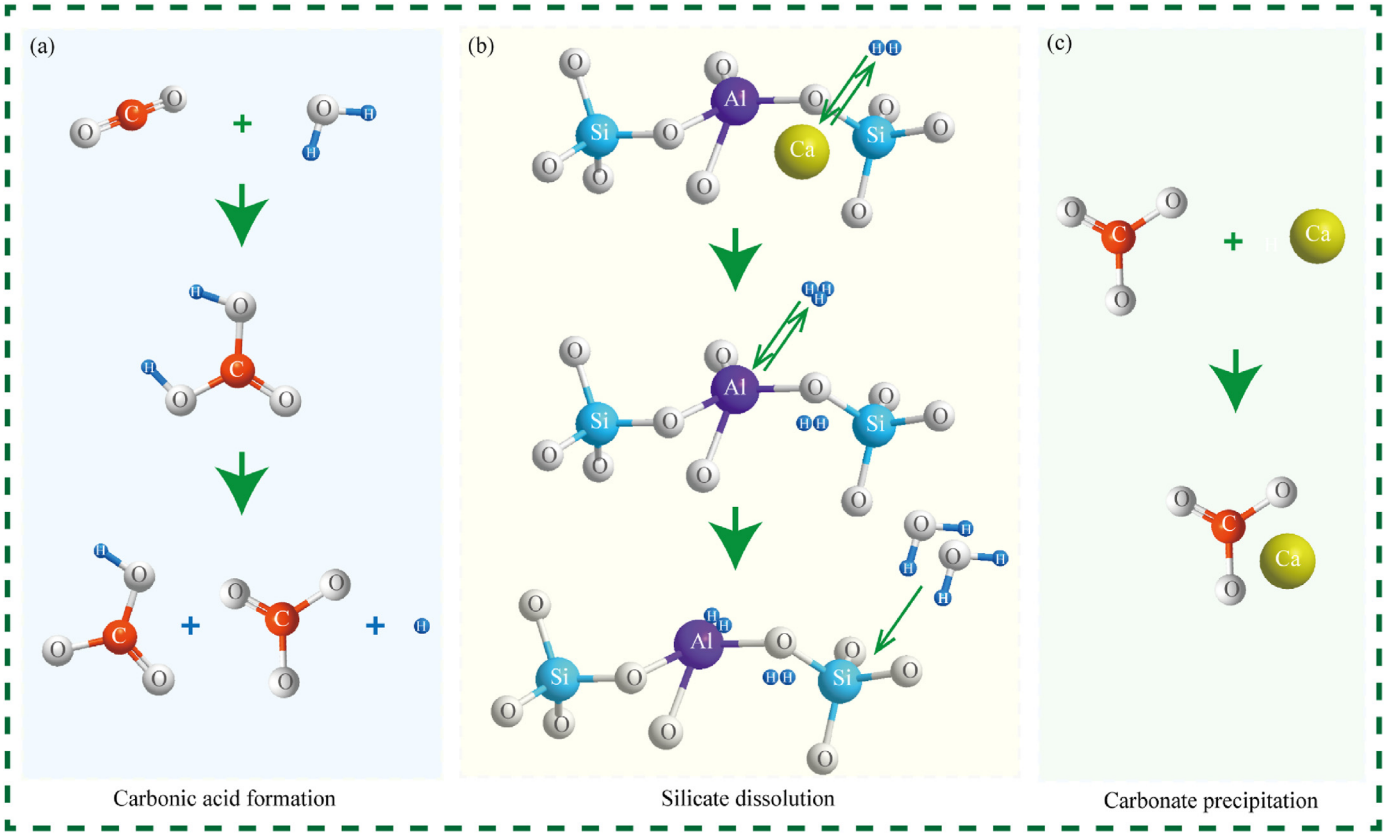

Fig. 2. Schematic diagram of carbon mineralization process (adapted from Oelkers and Gislason, 2001).

after the breaking of the monovalent and divalent metal-O bonds. Since the liberation of Si—O bonds is the rate-limiting step for silicate dissolution, the dissolution rate of silicate is often determined by the release rate of Si under far-from-equilibrium conditions (Shen et al., 2021). Several studies have proposed dissolution rate equations applied to various minerals, as shown in Table 2. Among them, a single oxide mineral indicates the dissolution process only requires destroying one type of metal-O bond, while the dissolution of a multi-oxide mineral necessitates the disruption of more than one type of metal-O bond (Schott et al., 2009).

Where r represents the far-from-equilibrium dissolution rate, a_i corresponds to the activity of the subscripted aqueous species, n refers to the order of dissolution reaction and k signifies the rate constant derived from Arrhenius' formula, which describes the correlation of the chemical reaction rate constant with the temperature (Liu, 2017):

$$k = A\exp\left(-\frac{E_a}{RT}\right) \tag{3}$$

where A is the preexponential factor, E_a denotes the reaction activation energy (kJ/mol), and R and T are the molar gas constant (kJ/(mol K)) and absolute temperature (K), respectively.

(3) Carbonate precipitation: The divalent cations react with dissolved CO_2 to generate stable carbonate mineral precipitation.

Table 2
The equations of dissolution rate for different silicate minerals.

No.	The equations of dissolution rate	Applications	References
1	$r = ka_{H^+}^n$	Single oxide mineral	(Guy and Schott, 1989; Hänchen et al., 2006)
2	$r = k(a_{H^+}^2/a_{M^{2+}})^n$	Multi-oxide silicate mineral and glass	Oelkers (2001)
3	$r = k(a_{H^+}^3/a_{Al^{3+}})^n$	Aluminosilicate minerals	(Gudbrandsson et al., 2014; Oelkers et al., 1994)
4	$r = k(a_{H^+}^3/a_{Al^{3+}})^{1/n}$	Aluminosilicate glass	Oelkers and Gislason (2001)

$$Ca^{2+}, Mg^{2+}, Fe^{2+} + CO_2 + H_2O \rightleftarrows (Ca, Mg, Fe)CO_3 + 2H^+ \tag{4}$$

The precipitation of carbonate minerals involves two distinct processes: nucleation and growth. The nucleation rate controls the mineral nucleation process which depends on the size and solubility of the crystal nucleus (Wu et al., 2022). According to classical nucleation theory, nucleation occurs when the grain size of the crystal nucleus is equal to the critical particle size. If the crystal nucleus is greater than the critical particle size, the crystal will grow; otherwise, dissolution will occur. From a thermodynamic perspective, mineral nucleation requires overcoming the nucleation barrier, which is the sum of the bulk phase energy (negative) and interfacial energy (positive) (Liu, 2017). Nucleation also

requires a critical degree of supersaturation, and when the nucleation rate is high, the dependence of the growth rate on supersaturation decreases (Pham et al., 2011; Wolthers et al., 2012).

It is generally believed that the dissolution rate of silicate minerals is lower than the precipitation rate of carbonate minerals so that the carbon mineralization reaction is controlled by the dissolution reaction of silicate minerals (Marini, 2007; Matter and Kelemen, 2009; Oelkers et al., 2008).

2.3. Experimental methodology

Laboratory experiments are fundamental to comprehending the carbon mineralization process and mechanism. At present, laboratory investigations on basalt carbonation reactions are principally conducted through batch reactions (Fig. 3a) or flow-through/flooding experiments (Fig. 3b), with mineral powder or intact core samples. The static batch apparatus is commonly used to study the long-term reaction, which provides a means to investigate the CO_2 mineralization mechanism and determine the possible carbonation products and reaction extent (Gysi and Stefánsson, 2012b; Wells et al., 2017a). Typically, this apparatus includes a gas entry, reactor vessel, and sampling. Samples are placed inside the reactor vessel at the designed temperature and pressure under no-flow conditions that are representative of diffusion-dominated regions (King et al., 2010). After a period, solid and solution are taken out and analyzed to evaluate the changes in rock mineralogy (Hellevang et al., 2017; Kumar et al., 2017), fluid compositions (Galeczka et al., 2014; Rosenqvist et al., 2023), pore structure (Hövelmann et al., 2012; Kanakiya et al., 2017) and mechanical properties (Adam et al., 2013; Guha Roy et al., 2016). In contrast, the flow-through apparatus is designed to replicate advection-controlled situations (Menefee et al., 2018; Peuble et al., 2015b), wherein fluid flow, solute transport and chemical reactions are considered. This apparatus consists of a gas entry, core holder, confining pressure and back pressure. Alternatively, it can integrate nuclear magnetic resonance (NMR) (Kanakiya et al., 2017; Wells et al., 2017b) or computed tomography (CT) (Phukan et al., 2021a; Xiong et al., 2018) to evaluate the evolution of pore structure and permeability throughout the whole testing process.

3. Carbon trapping mechanism

Under ideal conditions, all injected CO_2 is permanently sequestrated in the basalt reservoirs as carbonates. Nevertheless, due to the complex CO_2-fluid-basalt interaction, the products are frequently accompanied by other minerals, such as clay, chlorite and zeolite. In addition to injecting CO_2 at a certain pressure, many studies have also performed the reaction of basalt with carbonate or bicarbonate solution to mimic the phase when most protons have been consumed and aqueous CO_2 has been converted to carbonate alkalinity (Hellevang et al., 2017; Menefee et al., 2018; Wolff-Boenisch and Galeczka, 2018). Table 3 summarizes the

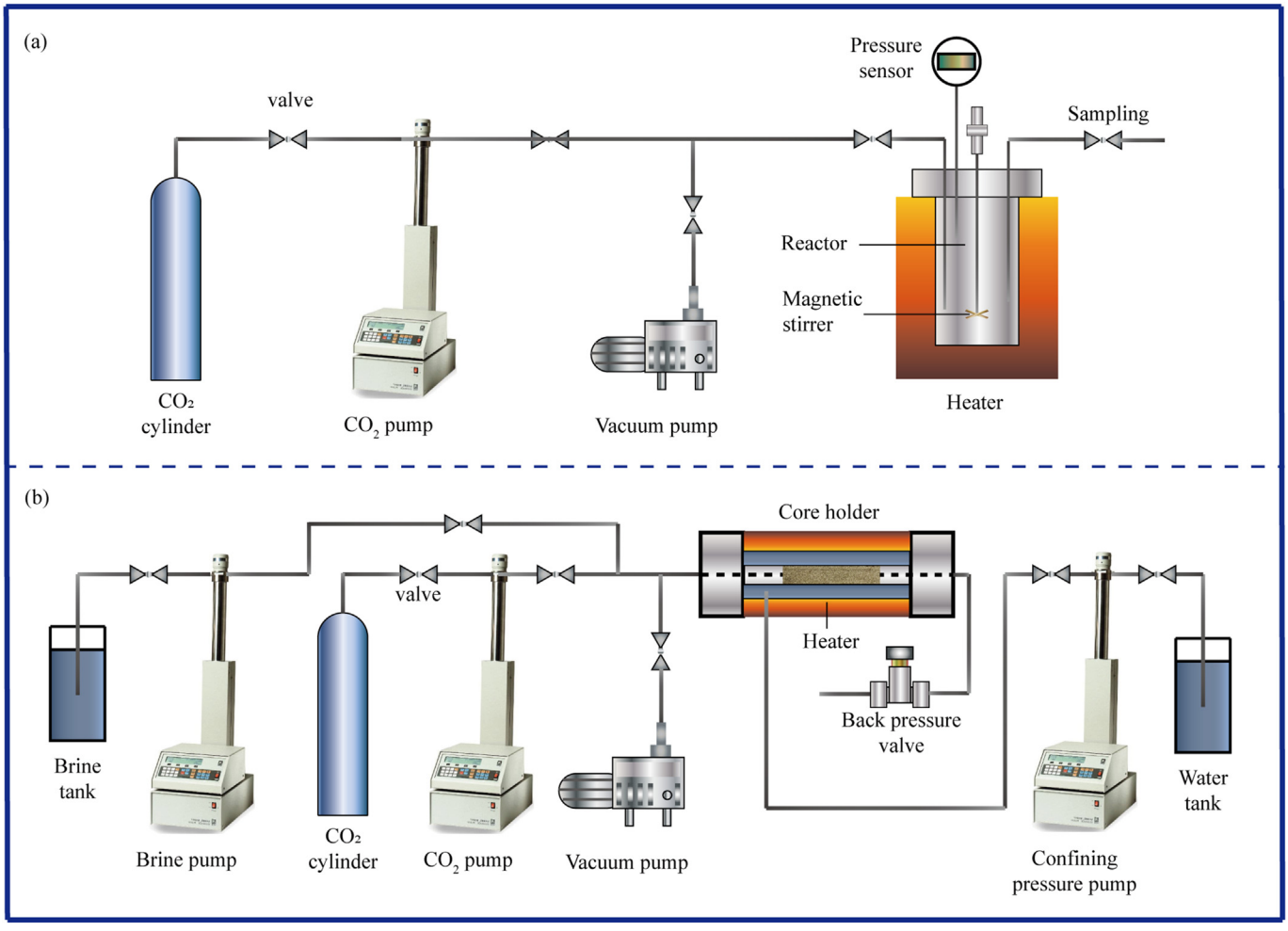

Fig. 3. Schematic diagram of the experimental setup. (a) Batch reactor apparatus and (b) Flow-through apparatus.

Table 3
Studies on CO_2-fluid-basalt reactions under different conditions.

Method	Primary minerals	Location	Sample size	Aqueous matrix	T (°C)	CO_2 pressure, p_{CO_2} (MPa)	Time	Secondary precipitates		References
								Carbonates	Others	
Batch reactor	Olivine	San Carlos (USA)	125–250 μm (size fraction)	0.01–0.25 mol/L $MgCl_2$ + 0.02–0.5 mol/L $NaHCO_3$	30–95	10	8–629 h	No	No	Giammar et al. (2005)
Batch reactor	Plagioclase, pyroxene and glass	CRB (USA)	0.42–2 mm (size fraction)	Pure water	100	10	225–1334 d	Calcite, siderite and magnesite	No	Schaef et al. (2009)
Batch reactor	Basaltic glass	Iceland	45–125 μm (size fraction)	Spring water	40	0.2–1.3	100 d	Ankerite	Smectite and ferrihydrite	Gysi and Stefánsson (2012a)
Batch reactor	Basaltic glass	Iceland	45–125 μm (size fraction)	Spring water	75–250	1.12–2.39	124 d	Ankerite, dolomite and calcite	Smectite, chlorite, zeolite, pyrite and amorphous silica	Gysi and Stefánsson (2012b)
Batch reactor	Plagioclase, pyroxene and olivine	Juan de Fuca Ridge (USA)	75–150 μm (size fraction)	0.5–1 mol/L NaCl	50–200	30	4300 h	Fe-bearing magnesite	No	Rosenbauer et al. (2012)
Batch reactor	Plagioclase, pyroxene and olivine	The Western Snake River Plain (USA)	2.5 cm × 3.8 cm (diameter × length)	Basalt-equilibrated water	100	8.3	30 weeks	Fe–Mg carbonates	No	Adam et al. (2013)
Flow-through	Olivine	San Carlos (USA)	9 mm × 18 mm (diameter × length)	Artificial seawater	190	19	23 d	No	Serpentine and hematite	Godard et al. (2013)
Batch reactor	Plagioclase, clinopyroxene, olivine, and glass	Iceland	33–80 μm (size fraction)	Pure water	150	28	2–45 d	Fe-bearing magnesite and minor calcite	Clay	Sissmann et al. (2014)
Flow-through	Olivine	Hawaii (USA)	6.35 mm × 13 mm (diameter × length)	0.57 mol/L $NaHCO_3$	180	10	55.8–92.4 h	Magnesite and Ca–Fe carbonates	Silica, iron oxide and serpentine	Peuble et al. (2015b)
Batch reactor	Plagioclase, clinopyroxene, olivine and glass	Decan (India)	54.7 mm (diameter)	Saturated sample	Room temperature	0.25	30–90 d	Calcite	Smectite	Guha Roy et al. (2016)
Batch reactor	Plagioclase, pyroxene, olivine and glass	CRB (USA)	2.54 cm × 4.2 cm (diameter × length)	1.2 mmol/L $NaHCO_3$ + 13.8 mmol/L NaCl	100	10	6 weeks	Siderite	Amorphous silica	Adeoye et al. (2017)
Batch reactor	Olivine	San Carlos (USA)	<53 μm (size fraction)	Pure water	150	10	28–56 d	Magnesite	Amorphous silica	Wells et al. (2017a)
Flow-through	Olivine	Cascade Range (USA)	1.84 cm × 3.81 cm (diameter × length)	Pure water and 0.6/1.5 mol/L $NaHCO_3$	150	10	3–7 d	Magnesite	Serpentine	Lisabeth et al. (2017)
Batch reactor	Basaltic glass	Iceland	63–125 μm (size fraction)	10 mmol/L Na_2CO_3	80–150		21–52 d	Ca-carbonates	Smectite	Hellevang et al. (2017)
Batch reactor	Plagioclase, pyroxene and olivine	Auckland (New Zealand)	2.5 cm × 3.31 cm (diameter × length)	Pre-equilibrated pure water	100	5.5	140 d	Ankerite	Clay/zeolite	Kanakiya et al. (2017)
Flow-through	Plagioclase, pyroxene and olivine	The Eastern Snake River Plain (USA)	1.3 cm × 2.6 cm (diameter × length)	1 mol/L NaCl	150	12.5	0.51–32.8 d	No	Fe oxide and clay	Luhmann et al. (2017)
Batch reactor	Plagioclase, clinopyroxene, olivine and glass	Iceland	45–125 μm (size fraction)	0.4–4 mol/L NH_4HCO_3 + artificial seawater	90		4.6–68 d	Calcite, magnesite and dawsonite-type carbonate	Clay, chlorite and zeolite	Wolff-Boenisch and Galeczka (2018)
Batch reactor	Plagioclase, pyroxene and glass	CRB (USA)	2.54 cm × 4 cm (diameter × length)	Pure water	100	10	6–40 weeks	Aragonite and calcite	Si-rich precipitate	Xiong et al. (2018)
Flow-through	Plagioclase, pyroxene, serpentine, and glass	Colorado (USA)	2.5 cm × 3.8 cm (diameter × length)	6.3–640 mmol/L $NaHCO_3$	100–150	10	12 d	Calcite, aragonite and Mg, Fe-bearing carbonates	Clay, Fe-oxide and amorphous silica	Menefee et al. (2018)
Batch reactor	Basaltic glass	Iceland	45–100 μm (size fraction)	Seawater and synthetic Mg-free seawater	130	0.25–1.6	2–228 d		Smectite and zeolite	Voigt et al. (2021)

Batch reactor	Plagioclase, feldspar, pyroxene and olivine	Victoria (Australia)	38 mm × 12 mm × 0.8 mm (length × width × thickness)	Artificial formation water	60	8	44 d	Calcite, aragonite, magnesite and minor siderite and ankerite No	Smectite, zeolite and Fe-oxide	Phukan et al. (2021b)
Batch reactor	Plagioclase, clinopyroxene, olivine and glass	Iceland	<63 μm (size fraction)	0.5 mol/L $NaHCO_3$	200–300		10 d	Calcite	Analcime and smectite	Kikuchi et al. (2023)
Batch reactor	Olivine	Henan province (China)	100 μm (average particle size)	Pure water	60	10	2.5–31 d	Magnesite and dolomite	Amorphous silica	Chen et al. (2023)

Table 4
The evolution of pore structure and permeability after the CO_2-fluid-basalt reaction.

Method	Sample	Aqueous matrix	Injection rate (mL/h)	T (°C)	p_{CO_2} (MPa)	Time	Porosity (%)		Permeability (mD)		References
							Before	After	Before	After	
Flow-through	Peridotite	1 mol/L NaCl + 0.6 mol/L $NaHCO_3$	36	160	11	(1) 200 min (2) 450 min	(1) 17 (2) 17	(2) 16.49–16.66	(1) 23 (2) 20	(1) 25 (2) 23	Andreani et al. (2009)
Batch reactor	Peridotite	Pure water		(1) 200 (2) 150 (3) 100	20	6 weeks	Average of 7.1	(1) 8.1 (2) 3.5 (3) 3.5			Hövelmann et al. (2012)
Batch reactor	Basalt	Basalt-equilibrated water		100	8.3	30 weeks	(1) 18.08 (2) 15.16	(1) 17.28 (2) 13.03	(1) 1.116 (2) 1.172	(1) 0.311 (2) 0.094	Adam et al. (2013)
Flow-through	Olivine	Artificial seawater	0.02–0.06	190	19	23 d	11.7	7.9–10.8	9.4×10^{-4}	8×10^{-5}	Godard et al. (2013)
Flow-through	Olivine	0.57 mol/L $NaHCO_3$	(1) 1 (2) 0.1	180	10	(1) 92.39 h (2) 55.8 h	(1) 6.15 (2) 6.02	(1) 5.5–5.7 (2) 5.8	(1) 0.33 (2) 4.1×10^{-2}	(1) 1.02×10^{-3} (2) 1.01×10^{-3}	Peuble et al. (2015b)
Flow-through	Olivine	(1) pure water (2) 0.6 mol/L $NaHCO_3$	Injection pressure = 10 MPa	150	0.8	7 d	1	(1) 1.1 (2) 1.07	(1) 0.63 (2) 0.13	(1) 0.32 (2) 0.02	Lisabeth et al. (2017)
Batch reactor	Basalt	Basalt-equilibrated water		100	5.5	142 d	(1) 48.3 (2) 19.5 (3) 17.6 (4) 11.1 (5) 4.9	(1) 63.6 (2) 21.3 (3) 17.9 (4) 13.1 (5) 13.2	(1) 9×10^{-3} (2) 1.9×10^{-3} (3) 2.3×10^{-2} (4) 10 (5) 5×10^{-3}	(1) 13.209 (2) 1.9×10^{-3} (3) 1.02×10^{-2} (4) 0.95 (5) 2.14×10^{-3}	Kanakiya et al. (2017)
Flow-through	Basalt	1 mol/L NaCl	(1) 6 (2) 6 (3) 0.6 (4) 0.6	150	12.5	(1) 0.51 d (2) 2.74 d (3) 19.62 d (4) 32.81 d	(1) 11.7 (2) 6.8 (3) 6.9 (4) 7.3	(1) 11 (2) 6.1 (3) 6.1 (4) 6.5	(1) 0.44 (2) 0.127 (3) 0.149 (4) 0.148	(1) 9.8 (2) 0.218 (3) 9.3×10^{-2} (4) 0.119	Luhmann et al. (2017)
Batch reactor	Basalt	Pure water		100	10	40 weeks	3.65	3.58			Xiong et al. (2018)
Batch reactor	Basalt	Pure water		60	8	12 weeks	9.75	9			Phukan et al. (2021a)
Batch reactor	Basalt	(1) alkaline solution (2) pure water (3) alkaline solution (4) alkaline solution (5) alkaline solution (6) pure water		30	6	(1) 24 h (2) 24 h (3) 48 h (4) 24 h (5) 48 h (6) 24 h	(1) 17.8 (2) 14.03 (3) 13.86 (4) 9.12 (5) 7.32 (6) 5.4	(1) 13.07 (2) 13.31 (3) 12.58 (4) 3.95 (5) 3.35 (6) 3.95	(1) 7245 (2) 3084 (3) 1380 (4) 36 (5) 19 (6) 13	(1) 36 (2) 11 (3) 89 (4) 4 (5) 3 (6) 2	Ye et al. (2022)

studies on CO_2-fluid-basalt reactions under different conditions. It can be seen there are differences in the produced secondary minerals under different reaction conditions even though the mineral compositions are similar. Therefore, the impact of the mineral compositions and the pore structure of the host rock, temperature, pH, CO_2 pressure, the chemical compositions of the formation water and the injected fluid, and other influcing factors are discussed, which helps to augment the conversion to carbonates and promote the mineralization rate.

3.1. Silicate dissolution

3.1.1. Mineral compositions and pore structure

Mineral compositions and pore structure are the primary factors determining the dissolution rate of silicate minerals. Generally speaking, both basaltic glass and crystalline basalt dissolve at a faster rate with lower silica content because Si–O bonds are more difficult to break than metal-O bonds (Wolff-Boenisch et al., 2004). Olivine has the fastest dissolution rate among the primary minerals of crystalline basalt, followed by pyroxene. However, at temperatures above 300 °C, the breaking of the Si–O bond becomes easier due to changes in water density and dielectric constant (Zhang et al., 2013). Basaltic glass, formed through rapid quenching in the diagenetic process, is less stable than the corresponding crystalline basalt (Gislason and Oelkers, 2003). Its dissolution rate is nearly the same as the dissolution rate of corresponding crystalline basalt at low silica content, but can reach twice that with high silica content (Wolff-Boenisch et al., 2006). A low dissolution rate of the glassy matrix was observed mainly resulting from its high Si:O ratio, which is almost 0.5 (Wells et al., 2017a). In addition to mineral compositions, the reaction surface area and pore structure of the minerals also have an impact on the dissolution rate. For fine particles, the specific surface area exposed to the reaction fluid is larger, and the dissolution rate is thus higher (Marieni et al., 2020). Similarly, host rocks with higher pore space and fractures have higher dissolution rates. Therefore, the selection of reservoirs with high reactivity and sufficient pore space is favorable for accelerating the carbon mineralization reaction process.

3.1.2. Temperature

Temperature plays a crucial role in the dissolution process of silicate minerals. According to Arrhenius' formula (Eq. (3)), the

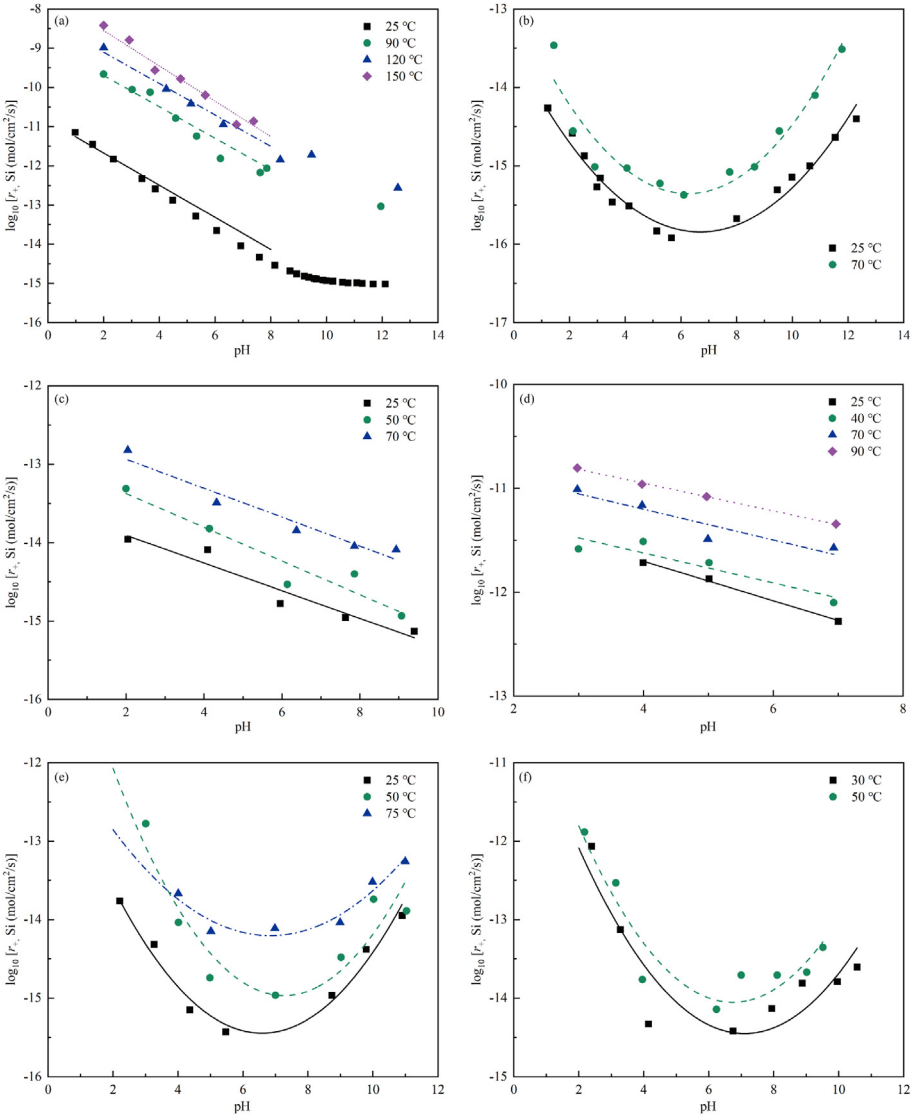

Fig. 4. The dissolution rates (r_+) of (a) forsterite, (b) albite, (c) diopside, (d) CRB, (e) Iceland basalt and (f) Iceland glass under different temperatures (Gislason and Oelkers, 2003; Gudbrandsson et al., 2011; Hänchen et al., 2006; Knauss et al., 1993; Pokrovsky and Schott, 2000; Schaef and McGrail, 2009; Schott et al., 2009).

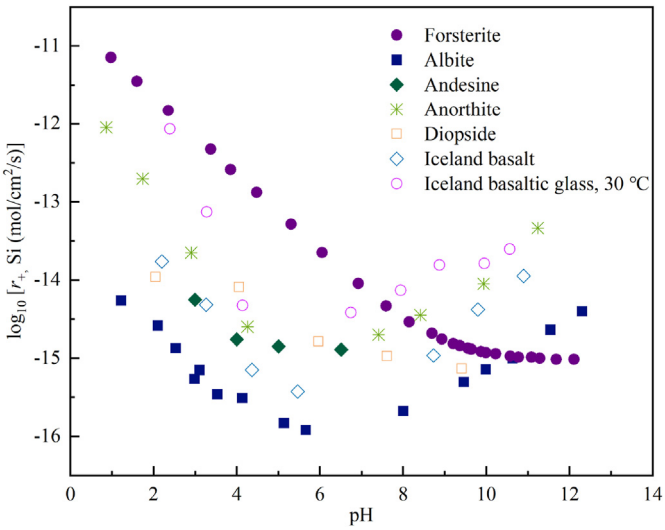

Fig. 5. The dissolution rates (r_+) of silicate minerals, basalt and basaltic glass with a wide range of pH values at 25 °C (Chou and Wollast, 1985; Gislason and Oelkers, 2003; Gudbrandsson et al., 2011, 2014; Knauss et al., 1993; Oxburgh et al., 1994; Pokrovsky and Schott, 2000).

chemical reaction rate constant increases with increasing temperature. In addition, the increased concentration of H^+ resulting from the dominance of carbonic acid dissociation at higher temperatures also contributes to the positive effect on the dissolution rate, as shown in Table 2 (Li et al., 2013). Fig. 4 displays the dissolution rates of several silicate minerals and basalt over a wide range of pH values at different temperatures. For identical minerals, the dissolution kinetics at different temperatures present similar pH-dependent patterns. All dissolution rates increased by approximately 0.5 log units when the temperature rose from 25 °C to 50 °C. When the temperature was elevated from 25 °C to 90 °C under both weakly acidic and neutral conditions, the CRB dissolution rate increased by 10 times (Schaef and McGrail, 2009) and the forsterite dissolution rate increased by nearly 100 times (Hänchen et al., 2006). Although temperature has a varying degree of influence on the silicate mineral dissolution, injecting the CO_2 into deeper formations is advantageous for expediting the dissolution process and subsequent release of divalent cations.

3.1.3. pH

The impact of pH on the dissolution rate of the silicate minerals is complex and displays variations depending on the specific type of mineral. Fig. 5 presents the dissolution rates of various silicate minerals, basalt and basaltic glass over a wide range of pH values at 25 °C, which exhibit either descending in a linear or parabolic fashion. Under acidic conditions, higher ion release rates are observed with a lower pH value, which can be ascribed to the higher activity of H^+ and the subsequent increase in diffusion exchange between divalent cations and H^+ and the surface protonation reaction (Eick et al., 1996). This finding is consistent with the dissolution rate equations, which describe a positive correlation between the dissolution rate and the H^+ activity. When the pH is between 6 and 7, the dissolution rates of the majority of minerals reach their minimum levels. At a higher pH, the dissolution rates of forsterite (Pokrovsky and Schott, 2000) and diopside (Knauss et al., 1993) decrease with an increasing pH, while the dissolution rates of albite (Chou and Wollast, 1985) and anorthite (Gudbrandsson et al., 2014) increase with an increasing pH. This is because the Al in aluminosilicates has amphoteric characteristics, enabling it to form complexes with OH^- under alkaline conditions. This reaction reduces the activity of Al^{3+}, thereby enhancing the dissolution rate (Xu et al., 2005). Moreover, basaltic glass dissolves fastest under neutral to alkaline conditions (Gíslason and Arnórsson, 1993).

The dissolution behavior of silicate minerals determines the release rate of the elements. Gudbrandsson et al. (2011) measured the crystalline basalt dissolution rate at a temperature of 25 °C and a pH ranging from 2 to 11. The release rates of Fe and Mg decreased with an increasing pH, which was consistent with the dissolution rates of olivine and diopside, while the release of Ca mainly came from the dissolution of plagioclase, leading to an initial decrease in its release rate followed by an increase as the pH increased. It is evident acidic conditions are more conducive to the dissolution of silicate minerals, and differences in mineral dissolution rates will further affect the preferential release of ions.

3.1.4. CO_2 pressure

It is generally believed the effect of CO_2 on the dissolution rate of silicate minerals is achieved by altering the pH value of the reaction system. In the study conducted by Prigiobbe et al. (2009), no direct relationship was found between the dissolution rate of olivine and the CO_2 pressure when the CO_2 pressure varied within the range of 0.2–10 MPa. Nevertheless, the logarithm of the olivine dissolution rate demonstrated a good negative linear relationship with the pH value. This indicates that the dissolution process is primarily influenced by the proton-promoting effect. Under higher CO_2 pressure, the pH is lower, and the concentration of dissolved H^+ is also higher, leading to a faster dissolution rate of the silicate minerals. Consequently, when the CO_2 pressure is not sufficient to affect the pH, the dissolution rate of the silicate minerals remains relatively unchanged (Brady and Carroll, 1994; Golubev et al., 2005). However, the logarithms of the Al release rates from anorthite present a positive correlation with the logarithms of the CO_3^{2-} concentrations (Berg and Banwart, 2000), which indicates CO_2 also has an accelerating effect by forming an Al-carbonate complex, commonly referred to as the complex-promoting effect. It remains unclear whether the CO_2 pressure itself has an impact on the dissolution rate of silicate minerals. Further research is required to gain a comprehensive understanding of the underlying mechanism of the CO_2 pressure effect.

3.1.5. Fluid chemistry

Formation water and seawater contain abundant salts and ions such as Ca^{2+}, Mg^{2+}, K^+, Na^+, Cl^-, SO_4^{2-}, CO_3^{2-} and HCO_3^-, which have complex influences on the silicate mineral dissolution process. Overall, the increased salinity favors the dissolution of the silicate minerals (Marieni et al., 2020; Wang and Giammar, 2013). Based on the dissolution rate of basaltic glass under salinities ranging from 0.035‰ to 3.5‰, parabolic growth and leveling off of the dissolution rate were observed with an increasing salinity (Morin et al., 2015). A salinity of 3.5‰ increased the dissolution rate by 3.5 times and this phenomenon is due to the increased dissolution rates of quartz and amorphous silica and the complex-promoting effect produced by some anions (Dove, 1999). Increased ionic strength also benefits the dissolution process due to the strengthened chemical polarity of the reaction solution, thus helping the polymerization of the aqueous H_4SiO_4 (Wang et al., 2019).

Excluding salinity and ionic strength, the salt type also controls the dissolution behavior of basalt. The mechanism behind Na^+, which is the most prevalent and extensively studied cation, is still a matter of debate. The batch experiments between San Carlos olivine powder and NaCl solution conducted by Wang and Giammar (2013) indicated an increase in the dissolution rate, which was enhanced by a factor of 27 with 0.87 mol/L NaCl after a reaction time of 1 month. They suggested the promoting effect was generated by Na^+ on or near the mineral surface in two aspects. On

the one hand, Na^+ promoted the Mg-proton exchange reaction. On the other hand, it facilitated the formation of aqueous H_4SiO_4 and its decomposition into amorphous silica, consequently removing the Si-rich layer. While the San Carlos olivine dissolution rate did not show any relationship with the sodium salt concentration even in the presence of 2.5 mol/L NaCl or $NaNO_3$ in the study by Prigiobbe et al. (2009). In contrast, observations from Stillings and Brantley (1995) argued the feldspar dissolution rate decreased with increasing NaCl concentration, which is attributed to the competition between Na^+ and H^+ for cation exchange sites. At present, the mechanism of fluid compositions on basalt dissolution is not clear and needs further study.

3.1.6. Other influencing factors

In addition to the factors mentioned above, other factors also play a non-negligible role in the dissolution process of basalt, but the mechanism necessitates further research. Organic ligands, such as acetate, citrate and oxalate, have been found to benefit basalt dissolution by promoting metal cation exchange adsorption through surface complexation (Franklin et al., 1994; Sun et al., 2023; Welch and Ullman, 1996). For instance, in Mg-silicates, negatively charged organic ligands attached to positively charged Mg atoms to form surface complexes and dissociated from the structure; meanwhile, protons attached to oxygen atoms and the Si–O structure was released (Olsen and Donald Rimstidt, 2008). The olivine dissolution rate with the addition of 0.001 mol/L ascorbic acid increased by 6 times at pH = 4 but only 2 times at pH = 2 (Wogelius and Walther, 1991). This is because the complex-promoting effect is pH-dependent and typically more pronounced at pH > 4 due to the reduction of hydrolyzed organic ligands under strongly acidic conditions (Liu et al., 2006). In addition, organic ligands exhibit varying chemical affinities for different cations (Perez et al., 2015). Oxalic acid and desferrioxamine preferentially adsorb on trivalent cations such as Al^{3+} and Fe^{3+}, while 2,2′-bipyridyl has a stronger complexation capacity with divalent cations such as Mg^{2+}, Fe^{2+} and Ca^{2+}. Similarly, fluoride can also promote the dissolution rate of silicate minerals through its complexation effect (Harouiya and Oelkers, 2004; Matter et al., 2011). An inference can be made that as the concentration of organic ligand or fluoride increases, the promotion effect on the dissolution rate becomes stronger, but there may exist a threshold. Simultaneously, suitable organic ligands should be selected for different silicate minerals to fully exploit the potential of enhancing dissolution rates.

The promoting effect of microorganisms on silicate mineral dissolution in the short term is well established, although the mechanism remains controversial. Some studies suggest that adhered bacteria display a complex-promoting effect on silicate mineral dissolution, which has a high affinity for polyvalent atoms. For example, *Pseudomonas aeruginosa* has been observed to attach to Fe(III), while *Paenibacillus polymyxa* prefers to break Al–O–Si bonds by complexing Al and Si atoms (Perez et al., 2019; Zhou et al., 2011). Different from breaking structural bonds, some other researches indicate microorganisms can accelerate dissolution by preventing the formation of an iron oxide passivation layer (Gerrits et al., 2020) or reducing the pH (Pokrovsky et al., 2021). However, during the long-term reaction processes, the growth of the microbial community on the mineral surface might limit the exchange adsorption of divalent cations, thereby inhibiting dissolution (Oelkers et al., 2015). Further research is necessary to understand the intricate mechanisms underlying the microbial facilitation of silicate mineral dissolution.

When injected at the industrial scale, CO_2 gas may contain impurity mixtures such as H_2S and SO_2. At the initial injection stage, the acidity of the reaction system is enhanced to some extent, favoring basalt dissolution. Under acidic environments, sulfate can also accelerate the dissolution of basalt and basaltic glass by forming a monodentate sulfate-Al complex (Flaathen et al., 2010). This complex has been discovered experimentally to enhance the anorthite dissolution rate by 1.36 times (Min et al., 2015). However, this promoting effect was nearly suppressed in the presence of oxalic acid, which can form a more stable bidentate complex. Notably, the role of CO_2 and salts should be accounted when investigating the complex-promoting effect.

3.2. Carbonate precipitation

3.2.1. Mineral compositions and pore structure

The mineral compositions and spatial distribution in host rocks are of great importance to the precipitation behavior of secondary minerals. In coarser-grained basalt, carbonates usually crystallize in clusters, while in finer-grained basalt, they are more uniformly distributed on the mineral surface in the form of small crystals (Adeoye et al., 2017). Interestingly, Ca-carbonate grains precipitated on pyroxene were larger than those on olivine due to the former being the primary Ca source, even on the same basalt (Menefee et al., 2018). Pore structure also plays a vital role in the precipitation of secondary minerals. Two olivine carbonation reaction experiments were designed in a static reactor and a nuclear magnetic resonance (NMR) reactor (Wells et al., 2017b). Analysis of the results revealed magnesite crystals tend to undergo heterogeneous nucleation and form independent particles or nodules in larger reactor volumes, while homogeneous nucleation usually occurs in smaller reactor volumes, resulting in fine-grained magnesite. Furthermore, preexisting fractures and large pores may act as diffusion-limited zones where preferential mineral precipitation occurs (Chen et al., 2023). These findings underscore the importance of considering the mineral compositions, the spatial distribution and the pore structure when studying secondary mineral precipitation in host rocks.

3.2.2. Temperature

Elevated temperatures favor the dissolution of silicate minerals, and thus more divalent cations are released. Meanwhile, the solubility of the CO_2 and the concentration of the CO_3^{2-} decrease. Many experimental studies have indicated basalt carbonation is more favorable at temperatures no higher than 100 °C. Higher temperatures can easily lead to the precipitation of secondary silicate minerals (Kumar and Shrivastava, 2020). Results from a series of basaltic glass carbonation experiments conducted at a pressure of 2 MPa and a temperature range of 75–250 °C revealed ankerite and dolomite were the main carbonation products at 75 °C (Gysi and Stefánsson, 2012b). However, at higher temperatures, only calcite was produced due to the incorporation of many divalent cations Mg^{2+} and Fe^{2+} by smectite and chlorite. Similarly, in a static reaction experiment between basalt and 0.5 mol/L $NaHCO_3$ solution at 200–300 °C, smectite occupied major divalent cations Mg^{2+} and Fe^{2+}, resulting in calcite as the only carbonate product (Kikuchi et al., 2023). Carbon mineralization experiments carried out at 30 MPa and 50–200 °C, however, did not observe the formation of clay minerals, and the reaction product was iron-bearing magnesite (Rosenbauer et al., 2012). Higher CO_2 pressure may have contributed to this observation. However, analysis of the experimental results suggested the reaction extent was still highest at 100 °C, with the amount of CO_2 uptake being four and five times the amount of CO_2 uptake at higher temperature and lower temperature, respectively. Additionally, increasing temperature can reduce the solubility of carbonate minerals, thus increasing the degree of carbonation (Bénézeth et al., 2011; Weyl, 1959).

Particularly, among the divalent cations, Mg^{2+} has a strong hydration property due to the high specific surface area charge and

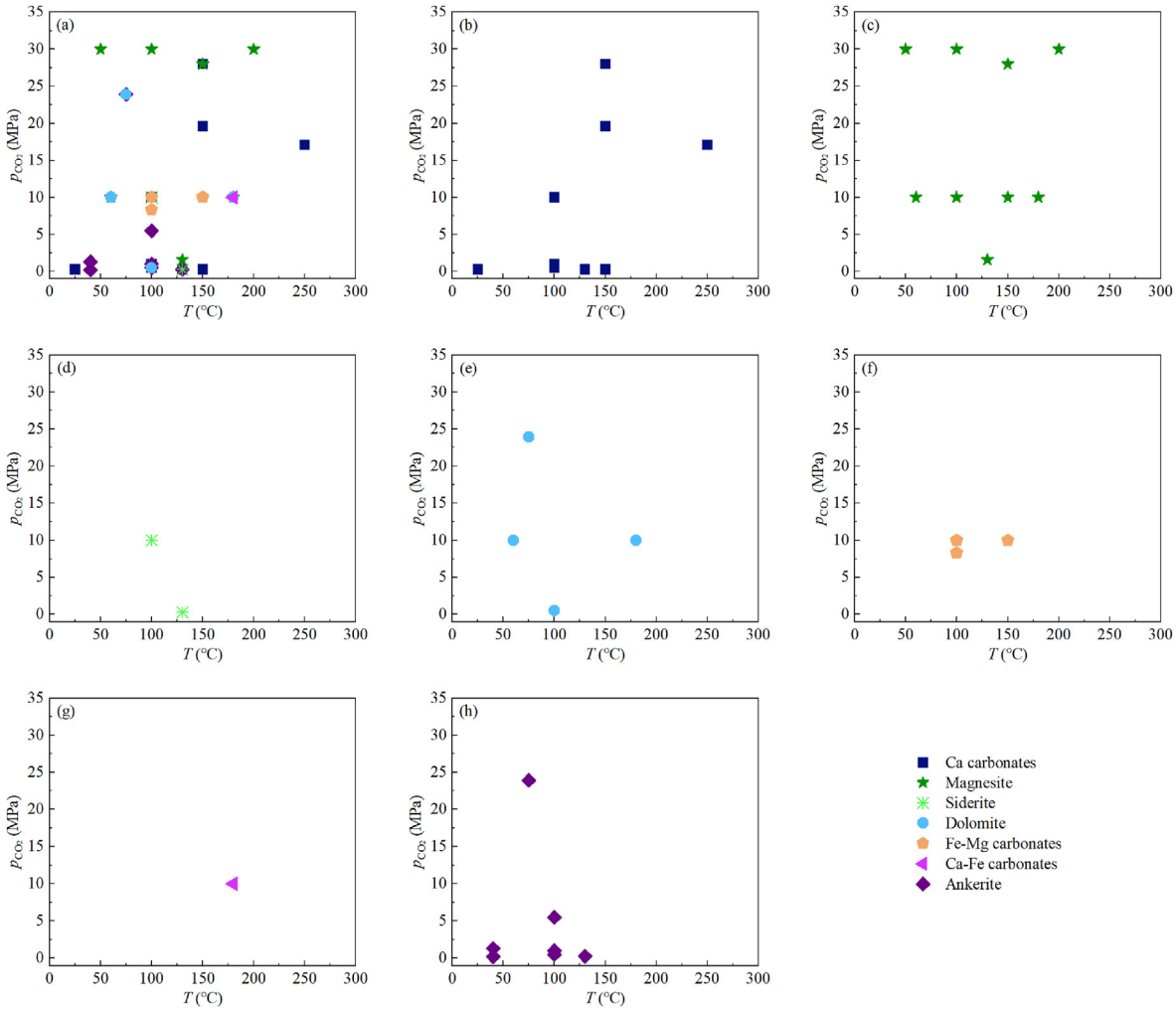

Fig. 6. The carbonate minerals formed under different temperatures and pressures (Adam et al., 2013; Adeoye et al., 2017; Chen et al., 2023; Guha Roy et al., 2016; Gysi and Stefánsson, 2012a, 2012b; Kanakiya et al., 2017; Kumar et al., 2017; Lisabeth et al., 2017; Menefee et al., 2018; Peuble et al., 2015b; Rosenbauer et al., 2012; Schaef et al., 2009; Sissmann et al., 2014; Voigt et al., 2021; Wells et al., 2017a; Xiong et al., 2018).

often bonds H_2O molecules to form metastable hydrous Mg-carbonates at low temperatures, such as nesquehonite ($MgCO_3 \cdot 3H_2O$), lansfordite ($MgCO_3 \cdot 5H_2O$) and hydromagnesite ($(MgCO_3)_4\ Mg(OH)_2 \cdot 4H_2O$) (Hänchen et al., 2008), which inhibit the precipitation of stable magnesite. The elevated temperature is beneficial to the dehydration process of Mg^{2+} (Prigiobbe and Mazzotti, 2013). Furthermore, the nucleation temperature of magnesite should be greater than 50 °C (Montes-Hernandez and Renard, 2016). In general, increasing temperature can accelerate the dissolution and precipitation reaction rates, but when the temperature is too high, the rapid decline in CO_2 solubility will lead to the reduction of CO_3^{2-} in the solution, which will reduce the proportion of carbonate precipitations in the products and CO_2 storage efficiency. Therefore, it is crucial to inject CO_2 into formations with an appropriate temperature to optimize the basalt carbonation reactions.

3.2.3. pH

Injecting supercritical CO_2 or aqueous CO_2 into the target reservoir causes a sharp drop in pH, which gradually rises with the consumption of protons and the release of divalent cations during the process of silicate dissolution. During this phase, it is important to create favorable pH conditions for the precipitation of carbonate minerals. Under acidic conditions, the solubility of siderite is two orders of magnitude lower than other carbonate minerals, making it easier to reach the saturation state (Clark et al., 2019). At pH = 4.2, siderite precipitation was found on the surface of Colorado basalt (100 °C and 10 MPa) (Adeoye et al., 2017). In the diffusion-limited zone where the pH buffering capacity was stronger, the precipitation product was Ca-carbonate, with a higher pH about 5.5 (Menefee et al., 2018). Typically, the Fe-rich carbonates formed first, followed by Mg-carbonates and then Ca-carbonates with increasing pH. Under alkaline conditions, Ca-carbonate is known to be predominant (Gislason et al., 1993). Note that Fe is readily oxidized when the pH exceeds 5.5 (Gysi and Stefánsson, 2012a). Adequate pH buffering capacity of the host rock is required to create suitable alkalinity for carbonate mineral precipitation.

3.2.4. CO_2 pressure

The dissolution-precipitation process of minerals is thought to be influenced by CO_2 pressure by altering the pH of the reaction system. Batch experiments conducted on basaltic glass and spring water under different CO_2 pressures (0.2 MPa and 1.3 MPa) at a temperature of 40 °C provided insight into this phenomenon (Gysi and Stefánsson, 2012a). In the experiment charged with a CO_2 pressure of 1.3 MPa, ankerite, smectite and ferrihydrite precipitated

with pH < 6.5. However, only ferrihydrite was observed for the experiment charged with a CO_2 pressure of 0.2 MPa and a pH above 6.5.

Several studies also suggest CO_2 can influence the processes of mineral nucleation and growth by changing the stoichiometry (CO_3^{2-}/M^{2+}) activity ratio (Hänchen et al., 2008; Hellevang et al., 2017; Sayles and Fyfe, 1973). In the reaction of basalt with an ammonium bicarbonate solution of 40 mmol/L at 90 °C, the products were silicates and zeolite. However, dawsonite-type carbonate ($NH_4AlCO_3(OH)_2$) was also generated at a higher concentration of 400 mmol/L (Wolff-Boenisch and Galeczka, 2018). The pH difference between these two reaction systems was relatively small, but the CO_3^{2-} activity of the latter was one order of magnitude higher than the CO_3^{2-} activity of the former. Experimental results conducted on basalt powder and seawater at 130 °C demonstrated aragonite and smectite were produced when the CO_2 pressure was 0.25 MPa. Nevertheless, at 1.6 MPa, magnesite replaced these minerals as the dominant product, and the initial CO_2 mineralization was almost three times higher than the CO_2 mineralization at low CO_2 pressure (Voigt et al., 2021). In addition, the carbonate crystals formed at high CO_2 concentrations usually grow into larger grains (Přikryl et al., 2018). It follows that elevating the CO_2 pressure can increase the carbon mineralization rate and the proportion of carbonates in secondary minerals, thereby improving the efficiency of CO_2 mineralization storage.

Indeed, higher CO_2 pressure is associated with higher CO_3^{2-} activity and lower pH, both of which control the formation sequence of carbonates and clay minerals (Clark et al., 2019). The data displayed in Fig. 6 illustrates the carbonates formed under varying temperature and CO_2 pressure conditions. Ca-carbonates are the most common carbonates formed across a broad range of temperatures and CO_2 pressures, while Mg-rich carbonates are more likely to form at elevated temperatures and CO_2 pressures due to their strong hydration properties. Fe is often incorporated in Ca/Mg carbonates.

3.2.5. Fluid chemistry

Alkaline groundwater or seawater can improve the pH buffering capacity of the CO_2-fluid-basalt reaction system and provide a supportive environment for carbonate precipitation (Wolff-Boenisch, 2011). Remarkably, the temperature reacting with seawater should not exceed 150 °C, above which a conspicuous amount of anhydrite will be generated (Bischoff and Seyfried, 1978). In the reaction between basaltic glass and seawater, the formation of magnesite was observed, which was not produced when reacting with freshwater due to the presence of Mg^{2+} in seawater (Voigt et al., 2021).

Sodium salt was found to work well on the transformation process of hydrous Mg-carbonate to magnesite by reducing the activity of the water, thus making dehydration of Mg^{2+} easier (King et al., 2010). However, the generated magnesite hardly changed or even decreased when the concentration was excessive (Ji et al., 2022). In the presence of 1 mol/L $NaHCO_3$ and 1 mol/L NaCl, the olivine carbonation was increased by 15 times and 2 times, respectively (Gadikota et al., 2014). Under the same temperature and pressure conditions, 1 mol/L $NaHCO_3$ enhanced the carbonation of labradorite, anorthite and basalt by 3–5 times, while 1 mol/L NaCl presented no positive effect (Gadikota et al., 2020). Obviously, the ability of $NaHCO_3$ to promote carbonation is more significant than the ability of NaCl to promote carbonation. This is because Na^+ mainly works by accelerating the silicate dissolution and inhibiting the formation of a Si-rich layer, while HCO_3^- also contributes to buffering and providing carbon sources. Progressively increasing the $NaHCO_3$ concentration to 2 mol/L, however, slightly increased the olivine carbonation. The rationale was the limited availability of Mg^{2+} when the CO_3^{2-} concentration exceeded the Mg^{2+} concentration. Various ions have the potential to either accelerate or inhibit the precipitation rate, as well as modify the types of carbonates produced, and this requires more study.

3.2.6. Other influencing factors

The acceleration effect of organic ligands on silicate dissolution has been widely accepted, but the inhibition effect on carbonate growth has also been noted. First, ligand complexation limits the availability of divalent cations for carbonates. Second, the adsorption of ligands on the growth sites of carbonate reduces the kinetic rate constant of carbonate growth, thus hindering the precipitation of carbonate (Gautier et al., 2016). Furthermore, organic ligands have a positive effect on carbonate dissolution, especially at concentrations greater than 0.01 mol/L (Miller et al., 2014; Pokrovsky et al., 2009). The co-injection of SO_2 and H_2S with CO_2 usually leads to the precipitation of (hydrated) sulfates (Schaef et al., 2014) and pyrite (Snaebjornsdottir et al., 2017). It is unclear whether sulfates or pyrite has a passivation effect and whether carbonates can continue to form after SO_2 and H_2S are consumed.

The slow kinetics of nucleation predominantly control the process of carbonate precipitation. To overcome the kinetic limitation, several studies have proposed seeding with carbonate or oxide particles to accelerate the precipitation rate of carbonates. In fact, carbonates are also presented in basalt reservoirs as alteration products during the natural weathering process that occurs over a long geological period. Direct precipitation of magnesite seeds in a CO_2-saline-olivine reaction system has been observed, which significantly enhanced the precipitation rate (Giammar et al., 2005). This phenomenon was more prominent at higher temperatures (Swanson et al., 2014). The acceleration effect of carbonate seeds on the carbonation process of basalt was agreed upon by Voigt et al. (2021). However, they argued the acceleration effect was induced by increasing the pH buffering capacity and alkalinity of the reaction system since the calcite seeds dissolved initially. Analogously, the addition of MgO favored the formation of magnesite, but magnesite was formed by MgO hydration (Ji et al., 2022). Further research is needed to understand the seeding mechanism.

3.3. Secondary mineral coating

The mineral coatings appear to decrease the dissolution rate of the underlying mineral by reducing the reaction surface area. As the most common carbonation products, the effects of carbonate, silica and secondary silicate coatings on the reaction rate of the underlying mineral have been extensively studied, but they are still ambiguous. Fig. 7 illustrates some secondary mineral coatings deposited on the surface of the olivine. Crystalline carbonate precipitates (Fig. 7a) have little effect on the basalt carbonation rate due to their porous nature, which allow the interaction between minerals and bulk solution (Stockmann et al., 2011, 2013). The limited influence of separate amorphous silica layer (Fig. 7b) is also confirmed (Daval et al., 2009; Saldi et al., 2013). Previous research results suggest the passivation effect is related to the performance of structure matching. When the crystallographic structure of the newly formed mineral is similar to that of the underlying mineral, it tends to precipitate via epaxial growth and produce a significant passivation effect. Conversely, if the crystallographic structures are different, the secondary mineral will precipitate via random three-dimensional nucleation and growth, resulting in a weaker passivation effect or will hardly impact the dissolution rate of coated minerals (Cubillas et al., 2005). In contrast, the intergrowths of Si-rich layers with carbonates, iron oxides, iron oxyhydroxides, Fe-, Mg-, Al-bearing phyllosilicates and so on significantly reduce the

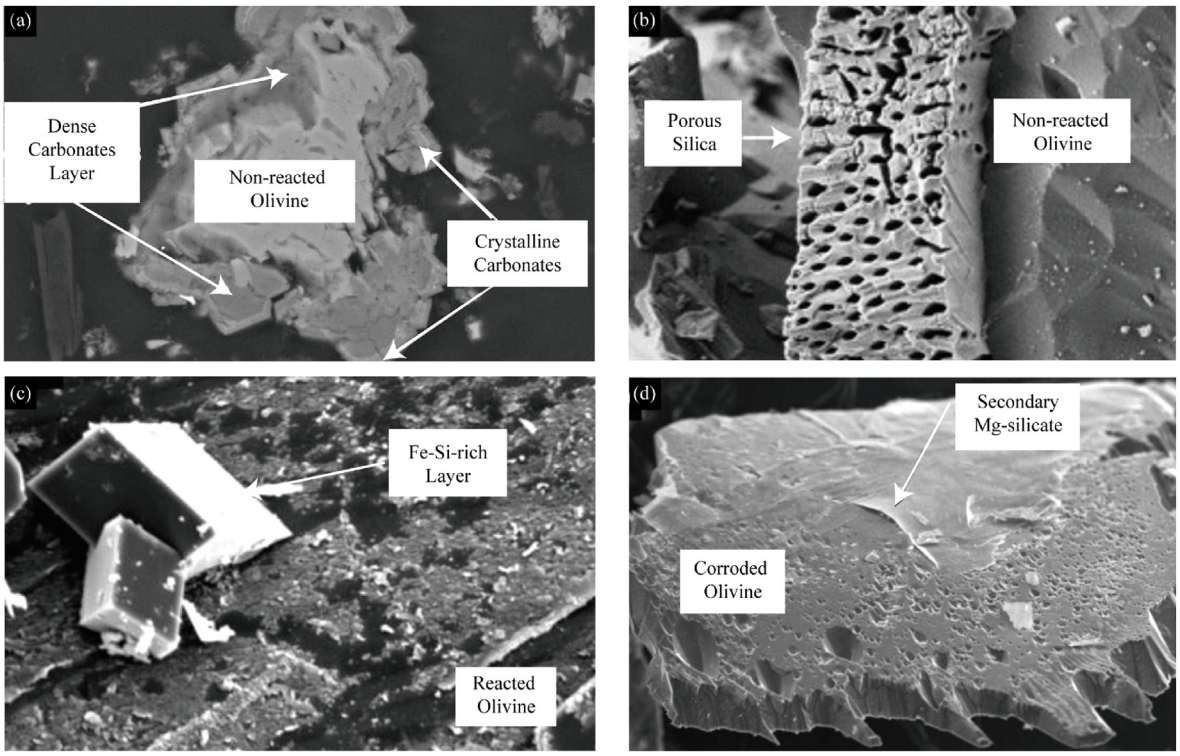

Fig. 7. Scanning electron microscope (SEM) images of secondary mineral precipitation (Bonfils et al., 2012; Saldi et al., 2013; Wang et al., 2019). (a) Crystallized carbonates and poorly crystallized, denser carbonates layer; (b) Highly porous silica layer; (c) Fe–Si-rich silica layer; (d) Thin sheet of Mg-silicate layer.

permeability of coating layers and passivate the underlying mineral even a thin layer (Fig. 7c) (Miller et al., 2019). Apart from crystallography and chemical compositions, a faster densification rate of the silica layer than olivine dissolution also contributes to the forming of a denser structure (Daval et al., 2011).

Particularly, when the CO_2 pressure is insufficient to completely crystallize the carbonates, a dense passivation layer (Fig. 7a) occurs (Wang et al., 2019). This indicates the initial conditions and rates of mineral nucleation and growth also have an impact on the microstructure of coating layers in addition to the precipitated matrix, thereby changing the porosity and permeability of the coating layers and controlling the dissolution rate of minerals (Arvidson and Mackenzie, 1999; Béarat et al., 2006). The passivation effect of secondary silicates has been widely recognized, as they act as an impermeable barrier (Fig. 7d) (Callow et al., 2018; Kumar and Shrivastava, 2020). At a temperature of 150 °C and CO_2 pressure of 28 MPa, basalt and olivine were reacted with pure water (Sissmann et al., 2014). After a month of reaction, both Fe-rich and Fe-poor magnesite were generated. Notably, the amount of the former was 2.5 times that of the latter. However, it is widely accepted that olivine has a faster reaction rate. This observation suggests that the Al- and Fe-bearing silica layer on the olivine surface has a more significant passivation effect compared to the clay minerals on the basalt surface.

The formation of a passivating layer may impair or even halt the carbonation reaction of the coated mineral. Mitigating the passivation effect of secondary mineral precipitation is of great significance for long-term basalt carbonation. One approach is to create new reaction surfaces through hydraulic fracturing or other methods. Additionally, selecting appropriate injection conditions also helps to avoid or minimize the formation of passivation layers. As mentioned in Section 3.2, decreasing the temperature and elevating the CO_2 pressure are favorable for reducing secondary silicate precipitation and relieving passivation effect. The passivation barriers were also overcome using organic acids in the study by Bonfils et al. (2012) and Sissmann et al. (2013). However, large amounts of Mg atoms were complexed by ligands, which had little effect on improving the carbonation extent. Therefore, developing more effective methods is needed.

4. Petrophysical and mechanical evolution

The interaction between CO_2-fluid-basalt not only causes changes in the mineral compositions, but also alters the pore structure, seepage characteristics and mechanical properties of the host rock, thus affecting the long-term injectivity and safety of carbon storage. In situ carbon mineralization storage requires sufficient pore volume and permeability for CO_2 injection and the precipitation of carbonates. Typically, mineral dissolution results in the dissolution and expansion of pores, throats and cracks, which may connect previously disconnected pores as well as generate new ones. This leads to an increase in porosity and permeability of the host rock. Mineral dissolution may also create new fractures in the reservoir, serving as leakage channels for CO_2 escape while simultaneously weakening the mechanical properties of the original rock. In contrast, mineral precipitation tends to clog pores, narrow throats and cracks, thus reducing porosity and permeability. This impedes further mineral exposure to the fluid while enhancing mechanical properties. Therefore, it is crucial to investigate the effect of CO_2-fluid-basalt reactions on the pore structure, permeability and the corresponding mechanical response of the host rock. Table 4 summarizes the experimental findings regarding the evolution of the pore structure and permeability after the CO_2-fluid-basalt reaction.

4.1. Pore structure and permeability

In static reaction experiments, the transport of reactive species is constrained and governed by diffusion. It is common to observe a decrease in permeability, while the response of porosity varies. The results of a series of high-temperature and high-pressure olivine carbonation experiments run by Hövelmann et al. (2012) reported porosity decreased with the progression of the carbonation reaction, and the change value was negatively linearly correlated with the degree of olivine carbonation. Analysis of backscattered electron images showed magnesite formed around olivine mineral particles and filled pores and fractures, which led to a decrease in the pore volume. Additionally, the precipitation rate increased with higher temperatures. Comparably, a 2%–3% reduction in porosity after the interaction of ferro-basalt with CO_2-rich water for 30 weeks was found, while the permeability was markedly reduced by 0.5-1 order of magnitude (Adam et al., 2013). Being different, five groups of basalt cores with different initial crystallinities, geometries and porosities were reacted with CO_2-rich water (Kanakiya et al., 2017). After 142 d, the porosity increased by 0.3%–15.3% although abundant ankerite and aluminosilicate minerals precipitates were found, suggesting a dissolution-dominated reaction. Permeability, however, showed a decreasing trend, primarily due to the localized precipitation of secondary minerals within the rock, resulting in a decrease in pore connectivity and blockage of the flow channels. In addition, spatial chemical gradients also led to variations in precipitation locations. Results from an experiment conducted on basalt with a prefabricated dead-end fracture occupying 0.2% of the core volume revealed that 5 mm^3 carbonates precipitated within the fracture, whereas only 7 mm^3 carbonates precipitated in the pore space of the entire rock. This finding indicated preferential transport occurred within the fracture so that more carbonates deposited in the region closer to the dead-end of the fracture with higher cation concentrations (Xiong et al., 2018).

Flow-through/flooding reaction experiments are more representative of the geological conditions in reservoirs than static reaction experiments. Reactive transport experiments effectively couple the kinetics of mineral dissolution-precipitation with the transport of fluid and solute, reflecting the competition in chemical reaction and fluid transport under varying injection rates. In a core flooding experiment performed by Godard et al. (2013) using olivine at an injection rate of no higher than 0.2 mL/h, it was discovered that olivine was already impermeable by 23 d, despite a decrease in porosity of less than 4%. Similarly, two reactive percolation experiments on olivine with injection rates of 0.1 mL/h and 1 mL/h also confirmed the drastic decline in permeability (Peuble et al., 2015b). At the higher flow rate, the permeability of the core decreased from 0.33 mD to 1.02×10^{-3} mD after 92 h, while it decreased from 4.1×10^{-2} mD to 1.01×10^{-3} mD at the lower flow rate with 56 h of displacement. However, the porosity only decreased by less than 1%. This finding suggests that the permeability decreases more pronounced than the porosity due to the heterogeneous distribution of flow paths. The localized precipitation of secondary minerals leads to blockage or closure of flow paths, thus causing a sharp decrease in permeability (Andreani et al., 2009), particularly at lower flow rates (Peuble et al., 2015a). In contrast, the experimental finding on basalt subjected to flow rates of 6 mL/h reported an increase in permeability of more than one order of magnitude, although porosity decreased (Luhmann et al., 2017). In fact, to some extent, the injection rate controls the permeability change. At low flow rates, the transport of fluid and solute is diffusion-controlled, allowing sufficient time for divalent cations to carbonize. This leads to a higher carbonation efficiency, but adversely, might result in the reduction of pore volume and

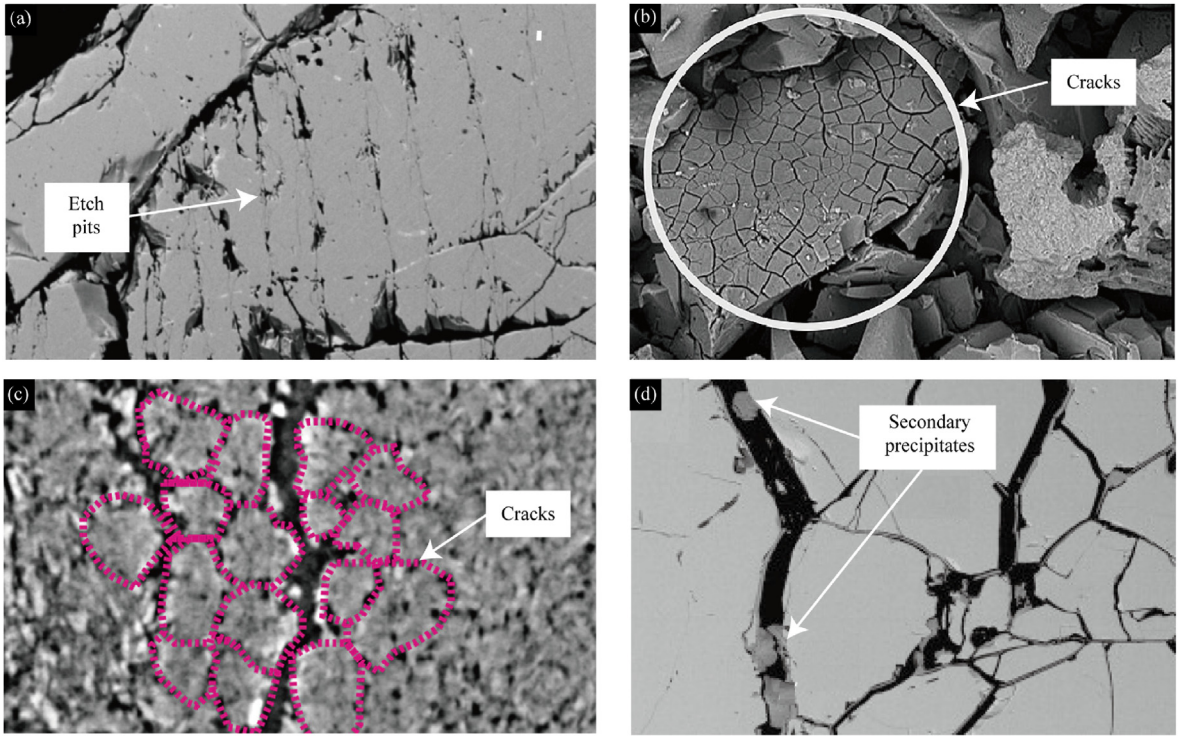

Fig. 8. Images of reaction-induced morphological changes under different physical and chemical processes (Hövelmann et al., 2012; Lisabeth et al., 2017; Přikryl et al., 2017; Zhu et al., 2016). (a) Etch pits developed by dissolution; (b) Cracks originated from dissolution; (c) Fracturing resulting from volume expansion; (d) The secondary minerals precipitated inside the cracks.

permeability. If all pores are filled instantaneously by precipitation, the porosity will disconnect sharply (Macente et al., 2022). In contrast, advection-controlled transport dominates at high flow rates. Since some divalent cations are carried away by the fluid without reacting, the carbonation efficiency is lower, and the damage to porosity reduction is also impaired. Whether dissolution-dominant or precipitation-dominant, the reactions are much more intense upstream (Luhmann et al., 2017; Peuble et al., 2015b), mainly resulting in a decrease in H^+ activity along the flow path. Also, the changes in porosity and permeability along the flow channels are often heterogeneous (Přikryl et al., 2017). In addition, the complete dissolution of minerals with smaller particles often results in the formation of etching pits, while mineral dissolution with larger particles usually results in micro-sized textures (Wells et al., 2017a).

The precipitation of secondary minerals in pores, throats and fractures of rock might obstruct the transport channels of fluid and solute, posing a threat to the long-term feasibility of CO_2 mineralization. Necessary rock modification methods are needed to improve the CO_2 injection capacity and carbon storage potential. To this end, microwave irradiation was used to increase the permeability of the cores, which resulted in 2–3 times more CO_2 mineralization (Ye et al., 2022). However, the rock modification in the study was carried out before the reaction, which would be more reasonable to evaluate the sustaining mineralization ability of the post-reacted cores.

4.2. Mechanical properties

The mechanical response of the basalt is closely related to the dissolution-precipitation reaction and the evolution of pore structure. In a study carried out by Guha Roy et al. (2016), saturated basalts were exposed to CO_2 of 0.25 MPa at room temperature for 30, 50, 70, and 90 d. A comprehensive evaluation of mechanical parameters suggested that the compressive strength, tensile strength, Young's modulus and shear modulus were all impaired with increasing reaction time, accompanied by a decline in P wave and S wave velocities. Meanwhile, newly formed cracks were observed along mineral boundaries and vesicles, indicating that dissolution was dominant. In contrast, the increment in ultrasonic wave velocities after the carbonation reaction of ferro-basalts for 30 weeks varied from 3.1% to 22%, which was attributed to the precipitation of carbonates in vesicles and cracks (Adam et al., 2013). Furthermore, the stress–strain curves of olivine interacting with pure water, 0.6 mol/L $NaHCO_3$ solution and 1.5 mol/L $NaHCO_3$ solution under hydrostatic pressure for approximately 72 h were measured by Lisabeth et al. (2017). The results revealed all samples exhibited localized brittle failure characteristics. Interestingly, the compressive strength of olivine reacting with $NaHCO_3$ solution was higher than the compressive strength of olivine reacting with pure water, but the Young's modulus was the opposite. This was due to the uneven precipitation of serpentine and magnesite within the cracks, which caused the self-sealing of cracks when reacting with $NaHCO_3$ solution (Phukan et al., 2021a), while a large amount of etch pits appeared in the sample reacting with pure water.

Of course, mineral precipitation does not always enhance mechanical properties. The crystallization pressure (Jamtveit et al., 2011; Kelemen and Hirth, 2012) or nonuniform volume expansion (Zhu et al., 2016) can sometimes fracture or even create collapse channels for CO_2 and impair the mechanical strength. However, no crystallization pressure has been observed during the basalt carbonation process. Fig. 8 displays the presence of reaction-induced etch pits, cracks, and secondary mineral fillings. The mechanical behavior also feeds back to chemical reactions. New crack spaces increase the reaction surface area exposed to CO_2-rich fluid and promote the mineral carbonation process, while the blockage of cracks or pore volume hinders further reaction. At present, the mechanical characterization of the basalt after a chemical reaction is still poorly understood, especially when initial cracks are present.

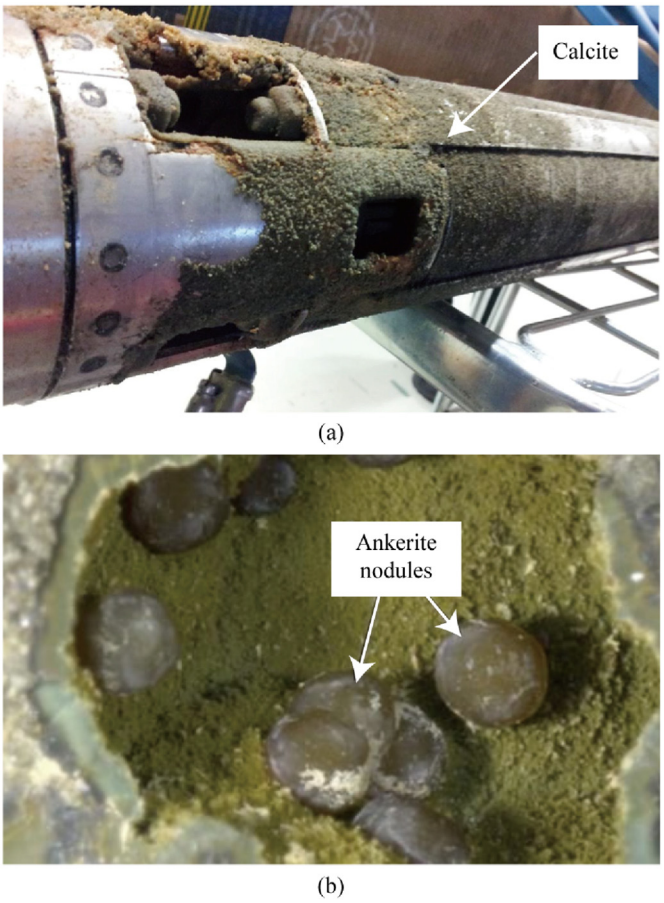

Fig. 9. Evidence of CO_2 mineralization (Polites et al., 2022; Snaebjornsdottir et al., 2017). (a) Calcite precipitation in the field of the CarbFix project; (b) Ankerite nodules in the field of the Wallula Pilot project.

5. Field pilot projects

The natural weathering process of basalt has proven to be effective in regulating the CO_2 level over geological time. Two pilot projects, CarbFix and Wallula, further demonstrate the feasibility of rapid CO_2 mineralization in basalt. In the CarbFix project, aqueous CO_2 was injected, while supercritical CO_2 was injected in the Wallula project. In comparison, injecting dissolved CO_2 greatly reduces the risk of leakage caused by CO_2 buoyancy. However, this method needs to consume a substantial amount of water, and the cost will increase. The details of these two pilots are discussed below.

5.1. The CarbFix pilot

The CarbFix pilot project is located 3 km south of the Hellisheidi geothermal power station in Iceland. The target injection formation is at a depth of 400–800 m, with a porosity of 8.5% and horizontal and vertical permeabilities of 300 and 1700 mD, respectively. The temperature ranges from 20 to 50 °C, and the pH is between 8.4 and 9.4 (Sigfusson et al., 2015). The chemical composition is olivine tholeiite, consisting of basaltic lava and hyaloclastite (Alfredsson

et al., 2008). From January 2012 to August 2012, a total of 175 t of pure CO_2 and 73 t of $CO_2 + H_2S + H_2$ mixtures were injected. The ^{14}C isotope was injected along with traditional tracers of volatile sulfur hexafluoride (SF_6) and trifluoromethyl sulfur pentafluoride (SF_5CF_3) to monitor the migration of CO_2. Calculations suggested CO_2 mineralization reached 95% within 2 years of injection, and the precipitation on the water sample pump was confirmed to be calcite (see Fig. 9a) (Matter et al., 2016; Snaebjornsdottir et al., 2017). The success of the CarbFix pilot project led to the upscaled CarbFix2 project, which has injection depths greater than 1300 m and temperatures greater than 250 °C (Clark et al., 2020). The injection began in 2014 and increased year by year, with the injection amount of CO_2 and H_2S accounting for 34% and 68% of total emissions until 2017 (Sigfússon et al., 2018).

5.2. The Wallula pilot

The Wallula Project is situated in the Columbia River Basalt in Wallula, Washington, USA. The target injection location is at 828–887 m and encompasses three brecciated flowtop and interflow zones. The flowtop is a medium permeability formation with a porosity of 15%–25% and a permeability of 75–150 mD, while the interflow layer has an extremely low permeability. The average temperature at the injection site is 36 °C (McGrail et al., 2011, 2017). It mainly consists of plagioclase, pyroxene and glass, with calcite and quartz filling veins, fractures and vesicles (McGrail et al., 2011). From July 2013 to August 2013, a total of 1000 t of supercritical CO_2 was injected. A perfluorocarbon tracer, perfluorodimethylcyclobutane (PFT), was also injected (McGrail et al., 2014). The fluid temperature survey showed most of the injected free CO_2 existed in the top interflow region, and the sidewall core revealed the formation of spherical carbonate nodules, which were identified as ankerite by X-ray diffraction (XRD) analysis (see Fig. 9b) (McGrail et al., 2017). It has been calculated mineralized CO_2 accounts for approximately 60% of the total injection amount after 2 years (White et al., 2020).

6. Conclusions and future work

In situ carbon mineralization in basalt is a safe, rapid and promising approach to achieve carbon neutrality. Accurately evaluating the carbon storage potential, carbon mineralization rate, long-term injectivity, and storage safety of a basalt reservoir, as well as accelerating the mineralization reaction rate necessitates a comprehensive understanding of the mechanisms of carbon mineralization. This work reviewed the factors influencing CO_2-fluid-basalt interaction, and the petrophysical and mechanical responses induced by basalt carbonation reaction based on laboratory experiments. The main conclusions and future work are as follows:

(1) High reactivity and sufficient pore space are the primary factors in choosing a reservoir. Given the acceleration effect of temperature, injecting CO_2 into deeper formations utilizing the geothermal gradient can enhance the rate of mineralization reaction. However, excessively high temperatures can generate secondary silicates, zeolites, gypsum, and other undesired products that are unfavorable for carbonate formation. Similarly, higher CO_2 pressure also promotes CO_2 mineralization, increases the proportion of carbonates in reaction products, and reduces water usage. It is worth noting that most of the existing studies focus on the carbonation process and products, thus more research is needed on the quantitative characterization of carbonation rate and carbonate conversion.

(2) The impact of fluid chemistry on CO_2 mineralization is still controversial and most of the experiments have been conducted with pure water or sodium salt solutions, but there is an growing interest in exploring the use of seawater due to its potential economic benefit, which is the future direction for implementing CO_2 storage in basalt. The effects of various ion components, salinity levels and ionic strengths should be fully considered and distinguished.

(3) Organic ligands, fluoride, microorganisms and gas mixtures have been reported to have a complex-promoting effect and benefit basalt dissolution, however, complexation also limits the availability of divalent cations for carbonates so that the acceleration effect needs further research.

(4) The passivation effect of secondary silicates and Si-rich layers' intergrowths with carbonates, iron oxides, iron oxyhydroxides, and Fe-, Mg-, Al-bearing phyllosilicates has been widely recognized, which greatly threatens the reactivity of the host rock. It is of great significance to study the mechanism of the passivation effect and how to weaken it.

(5) At lower flow rates, the transport of fluid and solute is diffusion-controlled, allowing sufficient carbonation time, which usually results in higher carbonation efficiency and the reduction of the pore volume and permeability. Conversely, advection-controlled transport dominates at higher flow rates. Some divalent cations are carried away by the fluid without reacting, resulting in lower carbonation efficiency but less damage to the porosity and permeability reduction. It is necessary to carry out reactive-percolation experiments under different injection rates, thus balancing carbonation efficiency and long-term CO_2 injectivity.

(6) The mechanical response is closely related to the dissolution and precipitation of minerals. A dissolution-controlled reaction commonly impairs the mechanical properties. When precipitation dominates, the sealing of pores, throats and cracks may lead to the strengthening of the mechanical properties, while the crystallization pressure or nonuniform volume expansion may also fracture the host rock. Research on chemo-mechanical coupling effect during carbon storage in basalt is expected. Considering the slow reaction rate, micromechanical test methods such as atomic force microscopy (AFM) and nanoindentation may provide insightful information.

Declaration of competing interest

The authors declare that they have no known competing financial interests or personal relationships that could have appeared to influence the work reported in this paper.

Acknowledgments

We acknowledge the funding support from the National Key R&D Program of China (Grant No. 2022YFE0115800), the Creative Groups of Natural Science Foundation of Hubei Province (Grant No. 2021CFA030), and Shanxi Provincial Key Research and Development Project (Grant No. 202102090301009).

References

Adam, L., van Wijk, K., Otheim, T., Batzle, M., 2013. Changes in elastic wave velocity and rock microstructure due to basalt-CO_2-water reactions. J. Geophys. Res. Solid Earth 118 (8), 4039–4047.

Adeoye, J.T., Menefee, A.H., Xiong, W., Wells, R.K., Skemer, P., Giammar, D.E., Ellis, B.R., 2017. Effect of transport limitations and fluid properties on reaction products in fractures of unaltered and serpentinized basalt exposed to high P_{CO2} fluids. Int. J. Greenh. Gas Control 63, 310–320.

Alfredsson, H.A., Hardarson, B.S., Franzson, H., Gislason, S.R., 2008. CO_2 sequestration in basaltic rock at the Hellisheidi site in SW Iceland: stratigraphy and chemical composition of the rocks at the injection site. Mineral. Mag. 72 (1), 1–5.

Amy, U., Wu, C.Z., Ji, J.F., Wang, Z.Y., Gu, L.X., Shu, P., Ding, R.X., 2012. Potential capacity and feasibility of CO_2 sequestration in petroleum reservoirs of basaltic rocks: example from basaltic hydrocarbon reservoir in the Xujiaweizi Fault Depression the Songliao Basin, East China. Geol. J. China Univ. 18 (2), 239–247 (in Chinese).

Andreani, M., Luquot, L., Gouze, P., Godard, M., Hoisé, E., Gibert, B., 2009. Experimental study of carbon sequestration reactions controlled by the percolation of CO_2-rich brine through peridotites. Environ. Sci. Technol. 43 (4), 1226–1231.

Anthonsen, K.L., Aagaard, P., Bergmo, P.E.S., Erlström, M., Fareide, J.I., Gislason, S.R., Mortensen, G.M., Snæbjörnsdottir, S.Ó., 2013. CO_2 storage potential in the Nordic region. Energy Proc. 37, 5080–5092.

Arvidson, R.S., Mackenzie, F.T., 1999. The dolomite problem; control of precipitation kinetics by temperature and saturation state. Am. J. Sci. 299 (4), 257–288.

Béarat, H., McKelvy, M.J., Chizmeshya, A.V.G., Gormley, D., Nunez, R., Carpenter, R.W., Squires, K., Wolf, G.H., 2006. Carbon sequestration via aqueous olivine mineral carbonation: role of passivating layer formation. Environ. Sci. Technol. 40 (15), 4802–4808.

Bénézeth, P., Saldi, G.D., Dandurand, J.-L., Schott, J., 2011. Experimental determination of the solubility product of magnesite at 50 to 200 °C. Chem. Geol. 286 (1), 21–31.

Berg, A., Banwart, S.A., 2000. Carbon dioxide mediated dissolution of Ca-feldspar: implications for silicate weathering. Chem. Geol. 163 (1), 25–42.

Bischoff, J.L., Seyfried, W.E., 1978. Hydrothermal chemistry of seawater from 25 degrees to 350 degrees C. Am. J. Sci. 278 (6), 838–860.

Bonfils, B., Julcour-Lebigue, C., Guyot, F., Bodénan, F., Chiquet, P., Bourgeois, F., 2012. Comprehensive analysis of direct aqueous mineral carbonation using dissolution enhancing organic additives. Int. J. Greenh. Gas Control 9, 334–346.

Bonto, M., Welch, M.J., Luthje, M., Andersen, S.I., Veshareh, M.J., Amour, F., Afrough, A., Mokhtari, R., Hajiabadi, M.R., Alizadeh, M.R., Larsen, C.N., Nick, H.M., 2021. Challenges and enablers for large-scale CO_2 storage in chalk formations. Earth Sci. Rev. 222, 103826.

Boschi, C., Dini, A., Dallai, L., Ruggieri, G., Gianelli, G., 2009. Enhanced CO_2-mineral sequestration by cyclic hydraulic fracturing and Si-rich fluid infiltration into serpentinites at Malentrata (Tuscany, Italy). Chem. Geol. 265 (1–2), 209–226.

Brady, P.V., Carroll, S.A., 1994. Direct effects of CO_2 and temperature on silicate weathering: possible implications for climate control. Geochem. Cosmochim. Acta 58 (7), 1853–1856.

Callow, B., Falcon-Suarez, I., Ahmed, S., Matter, J., 2018. Assessing the carbon sequestration potential of basalt using X-ray micro-CT and rock mechanics. Int. J. Greenh. Gas Control 70, 146–156.

Chen, M., Zhang, Y., Liu, S., Zhao, C., Dong, S., Song, Y., 2023. CO_2 transport and carbonate precipitation in the coupled diffusion-reaction process during CO_2 storage. Fuel 334, 126805.

Chou, L., Wollast, R., 1985. Steady-state kinetics and dissolution mechanisms of albite. Am. J. Sci. 285 (10), 963–993.

Clark, D.E., Galeczka, I.M., Diderikesen, K., Voigt, M.J., Wolff-Boenisch, D., Gislason, S.R., 2019. Experimental observations of CO_2-water-basaltic glass interaction in a large column reactor experiment at 50 degrees C. Int. J. Greenh. Gas Control 89, 9–19.

Clark, D.E., Oelkers, E.H., Gunnarsson, I., Sigfússon, B., Snæbjörnsdóttir, S.Ó., Aradóttir, E.S., Gíslason, S.R., 2020. CarbFix2: CO_2 and H_2S mineralization during 3.5 years of continuous injection into basaltic rocks at more than 250 °C. Geochem. Cosmochim. Acta 279, 45–66.

Cubillas, P., Köhler, S., Prieto, M., Causserand, C., Oelkers, E.H., 2005. How do mineral coatings affect dissolution rates? An experimental study of coupled $CaCO_3$ dissolution—$CdCO_3$ precipitation. Geochem. Cosmochim. Acta 69 (23), 5459–5476.

Daval, D., Martinez, I., Corvisier, J., Findling, N., Goffé, B., Guyot, F., 2009. Carbonation of Ca-bearing silicates, the case of wollastonite: experimental investigations and kinetic modeling. Chem. Geol. 265 (1), 63–78.

Daval, D., Sissmann, O., Menguy, N., Saldi, G.D., Guyot, F., Martinez, I., Corvisier, J., Garcia, B., Machouk, I., Knauss, K.G., Hellmann, R., 2011. Influence of amorphous silica layer formation on the dissolution rate of olivine at 90 °C and elevated pCO_2. Chem. Geol. 284 (1), 193–209.

Dove, P.M., 1999. The dissolution kinetics of quartz in aqueous mixed cation solutions. Geochem. Cosmochim. Acta 63 (22), 3715–3727.

Eick, M.J., Grossl, P.R., Golden, D.C., Sparks, D.L., Ming, D.W., 1996. Dissolution of a lunar basalt simulant as affected by pH and organic anions. Geoderma 74 (1), 139–160.

Flaathen, T.K., Gislason, S.R., Oelkers, E.H., 2010. The effect of aqueous sulphate on basaltic glass dissolution rates. Chem. Geol. 277 (3), 345–354.

Franklin, S.P., Hajash, A., Dewers, T.A., Tieh, T.T., 1994. The role of carboxylic acids in albite and quartz dissolution: an experimental study under diagenetic conditions. Geochem. Cosmochim. Acta 58 (20), 4259–4279.

Gadikota, G., Matter, J., Kelemen, P., Brady, P.V., Park, A.-H.A., 2020. Elucidating the differences in the carbon mineralization behaviors of calcium and magnesium bearing alumino-silicates and magnesium silicates for CO_2 storage. Fuel 277, 117900.

Gadikota, G., Matter, J., Kelemen, P., Park, A.-h.A., 2014. Chemical and morphological changes during olivine carbonation for CO_2 storage in the presence of NaCl and $NaHCO_3$. Phys. Chem. Chem. Phys. 16 (10), 4679–4693.

Galeczka, I., Wolff-Boenisch, D., Oelkers, E.H., Gislason, S.R., 2014. An experimental study of basaltic glass–H_2O–CO_2 interaction at 22 and 50 °C: implications for subsurface storage of CO_2. Geochem. Cosmochim. Acta 126, 123–145.

Gautier, Q., Bénézeth, P., Schott, J., 2016. Magnesite growth inhibition by organic ligands: an experimental study at 100, 120 and 146 °C. Geochem. Cosmochim. Acta 181, 101–125.

Gerrits, R., Pokharel, R., Breitenbach, R., Radnik, J., Feldmann, I., Schuessler, J.A., von Blanckenburg, F., Gorbushina, A.A., Schott, J., 2020. How the rock-inhabiting fungus *K. petricola* A95 enhances olivine dissolution through attachment. Geochem. Cosmochim. Acta 282, 76–97.

Giammar, D.E., Bruant, R.G., Peters, C.A., 2005. Forsterite dissolution and magnesite precipitation at conditions relevant for deep saline aquifer storage and sequestration of carbon dioxide. Chem. Geol. 217 (3–4), 257–276.

Gíslason, S.R., Arnórsson, S.n., 1993. Dissolution of primary basaltic minerals in natural waters: saturation state and kinetics. Chem. Geol. 105, 117–135.

Gislason, S.R., Oelkers, E.H., 2003. Mechanism, rates, and consequences of basaltic glass dissolution: II. An experimental study of the dissolution rates of basaltic glass as a function of pH and temperature. Geochem. Cosmochim. Acta 67 (20), 3817–3832.

Gislason, S.R., Veblen, D.R., Livi, K.J.T., 1993. Experimental meteoric water-basalt interactions: characterization and interpretation of alteration products. Geochem. Cosmochim. Acta 57 (7), 1459–1471.

Godard, M., Luquot, L., Andreani, M., Gouze, P., 2013. Incipient hydration of mantle lithosphere at ridges: a reactive-percolation experiment. Earth Planet Sci. Lett. 371–372, 92–102.

Goldberg, D.S., Takahashi, T., Slagle, A.L., 2008. Carbon dioxide sequestration in deep-sea basalt. Proc. Natl Acad. Sci. 105, 9920–9925.

Golubev, S.V., Pokrovsky, O.S., Schott, J., 2005. Experimental determination of the effect of dissolved CO_2 on the dissolution kinetics of Mg and Ca silicates at 25 degrees C. Chem. Geol. 217 (3–4), 227–238.

Gudbrandsson, S., Wolff-Boenisch, D., Gislason, S.R., Oelkers, E.H., 2011. An experimental study of crystalline basalt dissolution from $2 \leqslant pH \leqslant 11$ and temperatures from 5 to 75 °C. Geochem. Cosmochim. Acta 75 (19), 5496–5509.

Gudbrandsson, S., Wolff-Boenisch, D., Gislason, S.R., Oelkers, E.H., 2014. Experimental determination of plagioclase dissolution rates as a function of its composition and pH at 22 °C. Geochem. Cosmochim. Acta 139, 154–172.

Guha Roy, D., Vishal, V., Singh, T.N., 2016. Effect of carbon dioxide sequestration on the mechanical properties of Deccan basalt. Environ. Earth Sci. 75 (9), 771.

Guy, C., Schott, J., 1989. Multisite surface reaction versus transport control during the hydrolysis of a complex oxide. Chem. Geol. 78 (3), 181–204.

Gysi, A.P., Stefánsson, A., 2012a. CO_2-water-basalt interaction. Low temperature experiments and implications for CO_2 sequestration into basalts. Geochem. Cosmochim. Acta 81, 129–152.

Gysi, A.P., Stefánsson, A., 2012b. Mineralogical aspects of CO_2 sequestration during hydrothermal basalt alteration — an experimental study at 75 to 250 degrees C and elevated pCO_2. Chem. Geol. 306, 146–159.

Hänchen, M., Prigiobbe, V., Baciocchi, R., Mazzotti, M., 2008. Precipitation in the Mg-carbonate system—effects of temperature and CO_2 pressure. Chem. Eng. Sci. 63 (4), 1012–1028.

Hänchen, M., Prigiobbe, V., Storti, G., Seward, T.M., Mazzotti, M., 2006. Dissolution kinetics of fosteritic olivine at 90–150 °C including effects of the presence of CO_2. Geochem. Cosmochim. Acta 70 (17), 4403–4416.

Harouiya, N., Oelkers, E.H., 2004. An experimental study of the effect of aqueous fluoride on quartz and alkali-feldspar dissolution rates. Chem. Geol. 205 (1), 155–167.

Hellevang, H., Haile, B.G., Tetteh, A., 2017. Experimental study to better understand factors affecting the CO_2 mineral trapping potential of basalt. Greenh. Gas Sci. Technol. 7 (1), 143–157.

Hövelmann, J., Austrheim, H., Jamtveit, B., 2012. Microstructure and porosity evolution during experimental carbonation of a natural peridotite. Chem. Geol. 334, 254–265.

Iglauer, S., 2018. Optimum storage depths for structural CO_2 trapping. Int. J. Greenh. Gas Control 77, 82–87.

IPCC, 2022. Global Warming of 1.5 °C: IPCC Special Report on Impacts of Global Warming of 1.5 °C above Pre-industrial Levels in Context of Strengthening Response to Climate Change, Sustainable Development, and Efforts to Eradicate Poverty. Cambridge University Press, Cambridge, UK.

Jamtveit, B., Kobchenko, M., Austrheim, H., Malthe-Sorenssen, A., Royne, A., Svensen, H., 2011. Porosity evolution and crystallization-driven fragmentation during weathering of andesite. J. Geophys. Res. Solid Earth 116 (B12). https://doi.org/10.1029/2011JB008649.

Ji, Y., Madhav, D., Vandeginste, V., 2022. Kinetics of enhanced magnesium carbonate formation for CO_2 storage via mineralization at 200 °C. Int. J. Greenh. Gas Control 121, 103777.

Kanakiya, S., Adam, L., Esteban, L., Rowe, M.C., Shane, P., 2017. Dissolution and secondary mineral precipitation in basalts due to reactions with carbonic acid. J. Geophys. Res. Solid Earth 122 (6), 4312–4327.

Kelemen, P.B., Hirth, G., 2012. Reaction-driven cracking during retrograde metamorphism: olivine hydration and carbonation. Earth Planet Sci. Lett. 345–348, 81–89.

Kikuchi, S., Wang, J.J., Dandar, O., Uno, M., Watanabe, N., Hirano, N., Tsuchiya, N., 2023. $NaHCO_3$ as a carrier of CO_2 and its enhancement effect on mineralization during hydrothermal alteration of basalt. Front. Environ. Sci. 11, 1138007.

King, H.E., Plümper, O., Putnis, A., 2010. Effect of secondary phase formation on the carbonation of olivine. Environ. Sci. Technol. 44 (16), 6503–6509.

Knauss, K.G., Nguyen, S.N., Weed, H.C., 1993. Diopside dissolution kinetics as a function of pH, CO_2, temperature, and time. Geochem. Cosmochim. Acta 57 (2), 285–294.
Kumar, A., Shrivastava, J.P., 2019. Carbon capture induced changes in Deccan basalt: a mass-balance approach. Greenh. Gas Sci. Technol. 9 (6), 1158–1180.
Kumar, A., Shrivastava, J.P., 2020. Secondary silicates as a barrier to carbon capture and storage in Deccan basalt. Acta Geol. Sin. 94 (3), 861–876.
Kumar, A., Shrivastava, J.P., Pathak, V., 2017. Mineral carbonation reactions under water-saturated, hydrothermal-like conditions and numerical simulations of CO_2 sequestration in tholeiitic basalt of the Eastern Deccan Volcanic Province, India. Appl. Geochem. 84, 87–104.
Li, C.F., Zhao, X.T., Duan, W., Wu, T., Yao, Z.W., Chen, G.X., Li, G., Peng, X., 2022a. Strategic and geodynamic analyses of geo-sequestration of CO_2 in China offshore sedimentary basins. Chin. J. Theor. Appl. Mech. 55, 1–17 (in Chinese).
Li, P.C., Jiang, L.J., Cheng, J.H., Zhao, M.H., 2023. Assessment of carbon dioxide mineralization sequestration potential of volcanic rocks in Leizhou Peninsula, Guangdong Province, China. Geol. J. China Univ. 29 (1), 76–84 (in Chinese).
Li, Q., Liu, G.Z., Li, X.C., Chen, Z.A., 2022b. Intergenerational evolution and presupposition of CCUS technology from a multidimensional perspective. Adc. Eng. Sci. 54 (1), 157–166 (in Chinese).
Li, W.L., Xu, J.J., Jia, L.X., Ma, B., Chen, J., 2022c. Research progress on key technologies of CO_2 storage in basalts. Hydrogeol. Eng. Geol. 49 (3), 164–173 (in Chinese).
Li, X.Y., Chang, C., Yu, Q.C., 2013. Model of basalt dissolution rate under CO_2 mineral sequestration conditions. Geoscience 27 (6), 1477–1483 (in Chinese).
Lisabeth, H.P., Zhu, W., Kelemen, P.B., Ilgen, A., 2017. Experimental evidence for chemo-mechanical coupling during carbon mineralization in ultramafic rocks. Earth Planet Sci. Lett. 474, 355–367.
Liu, Y., Olsen, A.A., Rimstidt, D., 2006. Mechanism for the dissolution of olivine series minerals in acidic solutions. Am. Mineral. 91 (2–3), 455–458.
Liu, Z.M., 2017. Crystallization mechanisms in biomineralization and their applications. PhD Thesis. Zhejiang University, Hangzhou, Zhejiang, China (in Chinese).
Luhmann, A.J., Tutolo, B.M., Bagley, B.C., Mildner, D.F.R., Seyfried, W.E., Saar, M.O., 2017. Permeability, porosity, and mineral surface area changes in basalt cores induced by reactive transport of CO_2-rich brine. Water Resour. Res. 53 (3), 1908–1927.
Macente, A., Dobson, K.J., MacDonald, J., Wadsworth, F.B., Vasseur, J., 2022. The evolution of paleo-porosity in basalts: reversing pore-filling mechanisms using X-Ray computed tomography. Transp. Porous Media 145 (3), 697–717.
Marieni, C., Matter, J.M., Teagle, D.A.H., 2020. Experimental study on mafic rock dissolution rates within CO_2-seawater-rock systems. Geochem. Cosmochim. Acta 272, 259–275.
Marini, L., 2007. Geological Sequestration of Carbon Dioxide: Thermodynamics, Kinetics, and Reaction Path Modeling. Elsevier, Amsterdam, Netherlands.
Matter, J.M., Broecker, W.S., Gislason, S.R., Gunnlaugsson, E., Oelkers, E.H., Stute, M., Sigurdardóttir, H., Stefansson, A., Alfreðsson, H.A., Aradóttir, E.S., Axelsson, G., Sigfússon, B., Wolff-Boenisch, D., 2011. The CarbFix pilot project—storing carbon dioxide in basalt. Energy Proc. 4, 5579–5585.
Matter, J.M., Kelemen, P.B., 2009. Permanent storage of carbon dioxide in geological reservoirs by mineral carbonation. Nat. Geosci. 2 (12), 837–841.
Matter, J.M., Stute, M., Snaebjornsdottir, S.O., Oelkers, E.H., Gislason, S.R., Aradottir, E.S., Sigfusson, B., Gunnarsson, I., Sigurdardottir, H., Gunnlaugsson, E., Axelsson, G., Alfredsson, H.A., Wolff-Boenisch, D., Mesfin, K., Taya, D.F.D., Hall, J., Dideriksen, K., Broecker, W.S., 2016. Rapid carbon mineralization for permanent disposal of anthropogenic carbon dioxide emissions. Science 352 (6291), 1312–1314.
McGrail, B.P., Schaef, H.T., Ho, A.M., Chien, Y.J., Dooley, J.J., Davidson, C.L., 2006. Potential for carbon dioxide sequestration in flood basalts. J. Geophys. Res. Solid Earth 111 (B12). https://doi.org/10.1029/2005JB004169.
McGrail, B.P., Schaef, H.T., Spane, F.A., Cliff, J.B., Qafoku, O., Horner, J.A., Thompson, C.J., Owen, A.T., Sullivan, C.E., 2017. Field validation of supercritical CO_2 reactivity with basalts. Environ. Sci. Technol. Lett. 4 (1), 6–10.
McGrail, B.P., Spane, F.A., Amonette, J.E., Thompson, C.R., Brown, C.F., 2014. Injection and monitoring at the Wallula basalt pilot project. Energy Proc. 63, 2939–2948.
McGrail, B.P., Spane, F.A., Sullivan, E.C., Bacon, D.H., Hund, G., 2011. The Wallula basalt sequestration pilot project. Energy Proc. 4, 5653–5660.
Menefee, A.H., Giammar, D.E., Ellis, B.R., 2018. Permanent CO_2 trapping through localized and chemical gradient-driven basalt carbonation. Environ. Sci. Technol. 52 (15), 8954–8964.
Miller, Q.R.S., Kaszuba, J.P., Schaef, H.T., Thompson, C.J., Qiu, L., Bowden, M.E., Glezakou, V.A., McGrail, B.P., 2014. Experimental study of organic ligand transport in supercritical CO_2 fluids and impacts to silicate reactivity. Energy Proc. 63, 3225–3233.
Miller, Q.R.S., Schaef, H.T., Kaszuba, J.P., Gadikota, G., McGrail, B.P., Rosso, K.M., 2019. Quantitative review of olivine carbonation kinetics: reactivity trends, mechanistic insights, and research frontiers. Environ. Sci. Technol. Lett. 6 (8), 431–442.
Min, Y., Kubicki, J.D., Jun, Y.-S., 2015. Plagioclase dissolution during CO_2–SO_2 cosequestration: effects of sulfate. Environ. Sci. Technol. 49 (3), 1946–1954.
Mohammadian, E., Hadavimoghaddam, F., Kheirollahi, M., Jafari, M., Chenlu, X., Liu, B., 2023. Probing Solubility and pH of CO_2 in aqueous solutions: implications for CO_2 injection into oceans. J. CO_2 Util. 71, 102463.
Montes-Hernandez, G., Renard, F., 2016. Time-resolved in situ Raman Spectroscopy of the nucleation and growth of siderite, magnesite, and calcite and their precursors. Cryst. Growth Des. 16 (12), 7218–7230.
Morin, G.P., Vigier, N., Verney-Carron, A., 2015. Enhanced dissolution of basaltic glass in brackish waters: impact on biogeochemical cycles. Earth Planet Sci. Lett. 417, 1–8.
Oelkers, E.H., 2001. General kinetic description of multioxide silicate mineral and glass dissolution. Geochem. Cosmochim. Acta 65 (21), 3703–3719.
Oelkers, E.H., Arkadakskiy, S., Afifi, A.M., Hoteit, H., Richards, M., Fedorik, J., Delaunay, A., Torres, J.E., Ahmed, Z.T., Kunnummal, N., Gislason, S.R., 2022. The subsurface carbonation potential of basaltic rocks from the Jizan region of Southwest Saudi Arabia. Int. J. Greenh. Gas Control 120, 103772.
Oelkers, E.H., Benning, L.G., Lutz, S., Mavromatis, V., Pearce, C.R., Plümper, O., 2015. The efficient long-term inhibition of forsterite dissolution by common soil bacteria and fungi at Earth surface conditions. Geochem. Cosmochim. Acta 168, 222–235.
Oelkers, E.H., Gislason, S.R., 2001. The mechanism, rates and consequences of basaltic glass dissolution: I. An experimental study of the dissolution rates of basaltic glass as a function of aqueous Al, Si and oxalic acid concentration at 25 °C and pH = 3 and 11. Geochem. Cosmochim. Acta 65 (21), 3671–3681.
Oelkers, E.H., Gislason, S.R., Matter, J., 2008. Mineral carbonation of CO_2. Elements 4 (5), 333–337.
Oelkers, E.H., Schott, J., Devidal, J.-L., 1994. The effect of aluminum, pH, and chemical affinity on the rates of aluminosilicate dissolution reactions. Geochem. Cosmochim. Acta 58 (9), 2011–2024.
Olsen, A.A., Donald Rimstidt, J., 2008. Oxalate-promoted forsterite dissolution at low pH. Geochem. Cosmochim. Acta 72 (7), 1758–1766.
Oxburgh, R., Drever, J.I., Sun, Y.-T., 1994. Mechanism of plagioclase dissolution in acid solution at 25 °C. Geochem. Cosmochim. Acta 58 (2), 661–669.
Perez, A., Rossano, S., Trcera, N., Verney-Carron, A., Huguenot, D., van Hullebusch, E.D., Catillon, G., Razafitianamaharavo, A., Guyot, F., 2015. Impact of iron chelators on short-term dissolution of basaltic glass. Geochem. Cosmochim. Acta 162, 83–98.
Perez, A., Rossano, S., Trcera, N., Verney-Carron, A., Rommevaux, C., Fourdrin, C., Agnello, A.C., Huguenot, D., Guyot, F., 2019. Direct and indirect impact of the bacterial strain Pseudomonas aeruginosa on the dissolution of synthetic Fe(III)- and Fe(II)-bearing basaltic glasses. Chem. Geol. 523, 9–18.
Peuble, S., Andreani, M., Godard, M., Gouze, P., Barou, F., Van de Moortele, B., Mainprice, D., Reynard, B., 2015a. Carbonate mineralization in percolated olivine aggregates: linking effects of crystallographic orientation and fluid flow. Am. Mineral. 100 (2–3), 474–482.
Peuble, S., Godard, M., Luquot, L., Andreani, M., Martinez, I., Gouze, P., 2015b. CO_2 geological storage in olivine rich basaltic aquifers: new insights from reactive-percolation experiments. Appl. Geochem. 52, 174–190.
Pham, V.T.H., Lu, P., Aagaard, P., Zhu, C., Hellevang, H., 2011. On the potential of CO_2–water–rock interactions for CO_2 storage using a modified kinetic model. Int. J. Greenh. Gas Control 5 (4), 1002–1015.
Phukan, M., Jyoti, A., Black, J.R., Haese, R.R., 2021a. Changes in pore geometry and connectivity in the basalt pore network adjacent to fractures in response to CO_2-saturated fluid. Water Resour. Res. 57 (12), e2021WR030275.
Phukan, M., Vu, H.P., Haese, R.R., 2021b. Mineral dissolution and precipitation reactions and their net balance controlled by mineral surface area: an experimental study on the interactions between continental flood basalts and CO_2-saturated water at 80 bars and 60 degrees C. Chem. Geol. 559, 119909.
Pokrovsky, O.S., Golubev, S.V., Jordan, G., 2009. Effect of organic and inorganic ligands on calcite and magnesite dissolution rates at 60 °C and 30 atm pCO_2. Chem. Geol. 265 (1), 33–43.
Pokrovsky, O.S., Schott, J., 2000. Kinetics and mechanism of forsterite dissolution at 25 °C and pH from 1 to 12. Geochem. Cosmochim. Acta 64 (19), 3313–3325.
Pokrovsky, O.S., Shirokova, L.S., Zabelina, S.A., Jordan, G., Bénézeth, P., 2021. Weak impact of microorganisms on Ca, Mg-bearing silicate weathering. npj Mater. Degrad. 5 (1), 51.
Polites, E.G., Schaef, H.T., Horner, J.A., Owen, A.T., Holliman, J.E., McGrail, B.P., Miller, Q.R.S., 2022. Exotic carbonate mineralization recovered from a deep basalt carbon storage demonstration. Environ. Sci. Technol. 56 (20), 14713–14722.
Prigiobbe, V., Costa, G., Baciocchi, R., Hänchen, M., Mazzotti, M., 2009. The effect of CO_2 and salinity on olivine dissolution kinetics at 120 °C. Chem. Eng. Sci. 64 (15), 3510–3515.
Prigiobbe, V., Mazzotti, M., 2013. Precipitation of Mg-carbonates at elevated temperature and partial pressure of CO_2. Chem. Eng. J. 223, 755–763.
Příkryl, J., Jha, D., Stefánsson, A., Stipp, S., 2017. Mineral dissolution in porous media: an experimental and modeling study on kinetics, porosity and surface area evolution. Appl. Geochem. 87, 57–70.
Příkryl, J., Stefánsson, A., Pearce, C.R., 2018. Tracing olivine carbonation and serpentinization in CO_2-rich fluids via magnesium exchange and isotopic fractionation. Geochem. Cosmochim. Acta 243, 133–148.
Raza, A., Glatz, G., Gholami, R., Mahmoud, M., Alafnan, S., 2022. Carbon mineralization and geological storage of CO_2 in basalt: mechanisms and technical challenges. Earth Sci. Rev. 229, 104036.
Rosenbauer, R.J., Thomas, B., Bischoff, J.L., Palandri, J., 2012. Carbon sequestration via reaction with basaltic rocks: geochemical modeling and experimental results. Geochem. Cosmochim. Acta 89, 116–133.
Rosenqvist, M.P., Meakins, M.W.J., Planke, S., Millett, J.M., Kjøll, H.J., Voigt, M.J., Jamtveit, B., 2023. Reservoir properties and reactivity of the Faroe Islands basalt group: investigating the potential for CO_2 storage in the North Atlantic igneous Province. Int. J. Greenh. Gas Control 123, 103838.

Saldi, G.D., Daval, D., Morvan, G., Knauss, K.G., 2013. The role of Fe and redox conditions in olivine carbonation rates: an experimental study of the rate limiting reactions at 90 and 150 °C in open and closed systems. Geochem. Cosmochim. Acta 118, 157–183.
Sayles, F.L., Fyfe, W.S., 1973. The crystallization of magnesite from aqueous solution. Geochem. Cosmochim. Acta 37 (1), 87–99.
Schaef, H.T., Horner, J.A., Owen, A.T., Thompson, C.J., Loring, J.S., McGrail, B.P., 2014. Mineralization of basalts in the CO_2–H_2O–SO_2–O_2 system. Environ. Sci. Technol. 48 (9), 5298–5305.
Schaef, H.T., McGrail, B.P., 2009. Dissolution of Columbia River Basalt under mildly acidic conditions as a function of temperature: experimental results relevant to the geological sequestration of carbon dioxide. Appl. Geochem. 24 (5), 980–987.
Schaef, H.T., McGrail, B.P., Owen, A.T., 2009. Basalt–CO_2–H_2O interactions and variability in carbonate mineralization rates. Energy Proc. 1 (1), 4899–4906.
Schott, J., Pokrovsky, O.S., Oelkers, E.H., 2009. The link between mineral dissolution/precipitation kinetics and solution chemistry. Rev. Mineral. Geochem. 70 (1), 207–258.
Seifritz, W., 1990. CO_2 disposal by means of silicates. Nature 345 (6275), 486-486.
Shen, L.F., Dong, W.S., Wang, Z.L., Xu, Z.M., Zhu, W.M., 2021. Experimental study on the mass transfer-deterioration process of basalt under drying-wetting cycles and chemical reaction. Chin. J. Rock Mech. Eng. 40 (S1), 2662–2672.
Sigfússon, B., Arnarson, M.Þ., Snæbjörnsdóttir, S.Ó., Karlsdóttir, M.R., Aradóttir, E.S., Gunnarsson, I., 2018. Reducing emissions of carbon dioxide and hydrogen sulphide at Hellisheidi power plant in 2014-2017 and the role of CarbFix in achieving the 2040 Iceland climate goals. Energy Proc. 146, 135–145.
Sigfusson, B., Gislason, S.R., Matter, J.M., Stute, M., Gunnlaugsson, E., Gunnarsson, I., Aradottir, E.S., Sigurdardottir, H., Mesfin, K., Alfredsson, H.A., Wolff-Boenisch, D., Arnarsson, M.T., Oelkers, E.H., 2015. Solving the carbon-dioxide buoyancy challenge: the design and field testing of a dissolved CO_2 injection system. Int. J. Greenh. Gas Control 37, 213–219.
Sissmann, O., Brunet, F., Martinez, I., Guyot, F., Verlaguet, A., Pinquier, Y., Daval, D., 2014. Enhanced olivine carbonation within a basalt as compared to single-phase experiments: reevaluating the potential of CO_2 mineral sequestration. Environ. Sci. Technol. 48 (10), 5512–5519.
Sissmann, O., Daval, D., Brunet, F., Guyot, F., Verlaguet, A., Pinquier, Y., Findling, N., Martinez, I., 2013. The deleterious effect of secondary phases on olivine carbonation yield: insight from time-resolved aqueous-fluid sampling and FIB-TEM characterization. Chem. Geol. 357, 186–202.
Snæbjörnsdóttir, S.Ó., Gislason, S.R., 2016. CO_2 storage potential of basaltic rocks offshore Iceland. Energy Proc. 86, 371–380.
Snaebjornsdottir, S.O., Oelkers, E.H., Mesfin, K., Aradottir, E.S., Dideriksen, K., Gunnarsson, I., Gunnlaugsson, E., Matter, J.M., Stute, M., Gislason, S.R., 2017. The chemistry and saturation states of subsurface fluids during the in situ mineralisation of CO_2 and H_2S at the CarbFix site in SW-Iceland. Int. J. Greenh. Gas Control 58, 87–102.
Snaebjornsdottir, S.O., Sigfusson, B., Marieni, C., Goldberg, D., Gislason, S.R., Oelkers, E.H., 2020. Carbon dioxide storage through mineral carbonation. Nat. Rev. Earth Environ. 1 (2), 90–102.
Snæbjörnsdóttir, S.Ó., Wiese, F., Fridriksson, T., Ármansson, H., Einarsson, G.M., Gislason, S.R., 2014. CO_2 storage potential of basaltic rocks in Iceland and the oceanic ridges. Energy Proc. 63, 4585–4600.
Song, Y.S., Jun, S.J., Na, Y.S., Kim, K., Jang, Y., Wang, J.H., 2023. Geomechanical challenges during geological CO_2 storage: a review. Chem. Eng. J. 456, 140968.
Stillings, L.L., Brantley, S.L., 1995. Feldspar dissolution at 25 °C and pH 3: reaction stoichiometry and the effect of cations. Geochem. Cosmochim. Acta 59 (8), 1483–1496.
Stockmann, G.J., Wolff-Boenisch, D., Gislason, S.R., Oelkers, E.H., 2011. Do carbonate precipitates affect dissolution kinetics? 1: basaltic glass. Chem. Geol. 284 (3), 306–316.
Stockmann, G.J., Wolff-Boenisch, D., Gislason, S.R., Oelkers, E.H., 2013. Do carbonate precipitates affect dissolution kinetics? 2. Diopside. Chem. Geol. 337–338, 56–66.
Sun, C., Yao, Z., Wang, Q., Guo, L., Shen, X., 2023. Theoretical study on the organic acid promoted dissolution mechanism of forsterite mineral. Appl. Surf. Sci. 614, 156063.
Swanson, E.J., Fricker, K.J., Sun, M., Park, A.H.A., 2014. Directed precipitation of hydrated and anhydrous magnesium carbonates for carbon storage. Phys. Chem. Chem. Phys. 16 (42), 23440–23450.
Vishal, V., Verma, Y., Chandra, D., Ashok, D., 2021. A systematic capacity assessment and classification of geologic CO_2 storage systems in India. Int. J. Greenh. Gas Control 111, 103458.
Voigt, M., Marieni, C., Baldermann, A., Galeczka, I.M., Wolff-Boenisch, D., Oelkers, E.H., Gislason, S.R., 2021. An experimental study of basalt-seawater-CO_2 interaction at 130 degrees C. Geochem. Cosmochim. Acta 308, 21–41.
Wang, F., Dreisinger, D., Jarvis, M., Hitchins, T., 2019. Kinetics and mechanism of mineral carbonation of olivine for CO_2 sequestration. Miner. Eng. 131, 185–197.
Wang, F., Giammar, D.E., 2013. Forsterite dissolution in saline water at elevated temperature and high CO_2 pressure. Environ. Sci. Technol. 47 (1), 168–173.
Welch, S.A., Ullman, W.J., 1996. Feldspar dissolution in acidic and organic solutions: compositional and pH dependence of dissolution rate. Geochem. Cosmochim. Acta 60 (16), 2939–2948.
Wells, R.K., Xiong, W., Giammar, D., Skemer, P., 2017a. Dissolution and surface roughening of Columbia River flood basalt at geologic carbon sequestration conditions. Chem. Geol. 467, 100–109.
Wells, R.K., Xiong, W., Sesti, E., Cui, J.L., Giammar, D., Skemer, P., Hayes, S.E., Conradi, M.S., 2017b. Spatially-variable carbonation reactions in polycrystalline olivine. Geochem. Cosmochim. Acta 204, 252–266.
Weyl, P.K., 1959. The change in solubility of calcium carbonate with temperature and carbon dioxide content. Geochem. Cosmochim. Acta 17 (3), 214–225.
White, S.K., Spane, F.A., Schaef, H.T., Miller, Q.R.S., White, M.D., Horner, J.A., McGrail, B.P., 2020. Quantification of CO_2 mineralization at the Wallula basalt pilot project. Environ. Sci. Technol. 54 (22), 14609–14616.
Wogelius, R.A., Walther, J.V., 1991. Olivine dissolution at 25 °C: effects of pH, CO_2, and organic acids. Geochem. Cosmochim. Acta 55 (4), 943–954.
Wolff-Boenisch, D., 2011. On the buffer capacity of CO_2-charged seawater used for carbonation and subsequent mineral sequestration. Energy Proc. 4, 3738–3745.
Wolff-Boenisch, D., Galeczka, I.M., 2018. Flow-through reactor experiments on basalt-(sea)water-CO_2 reactions at 90 degrees C and neutral pH. What happens to the basalt pore space under post-injection conditions? Int. J. Greenh. Gas Control 68, 176–190.
Wolff-Boenisch, D., Gislason, S.R., Oelkers, E.H., 2006. The effect of crystallinity on dissolution rates and CO_2 consumption capacity of silicates. Geochem. Cosmochim. Acta 70 (4), 858–870.
Wolff-Boenisch, D., Gislason, S.R., Oelkers, E.H., Putnis, C.V., 2004. The dissolution rates of natural glasses as a function of their composition at pH 4 and 10.6, and temperatures from 25 to 74 degrees C. Geochem. Cosmochim. Acta 68 (23), 4843–4858.
Wolthers, M., Nehrke, G., Gustafsson, J.P., Van Cappellen, P., 2012. Calcite growth kinetics: modeling the effect of solution stoichiometry. Geochem. Cosmochim. Acta 77, 121–134.
Wu, K.Y., Xiong, Y., Tan, X.C., Liu, X.J., Zhang, Y.F., Chen, X.D., Li, Y.F., Guo, R.T., Cao, Z., Wang, P., 2022. Research progress of "water-rock" reaction crystallization kinetics for a pore system in a reservoir. Acta Sedimentol. Sin. 40 (4), 996–1009 (in Chinese).
Xiong, W., Wells, R.K., Horner, J.A., Schaef, H.T., Skemer, P.A., Giammar, D.E., 2018. CO_2 mineral sequestration in naturally porous basalt. Environ. Sci. Technol. Lett. 5 (3), 142–147.
Xu, L., Li, Q., Myers, M.B., Chen, Q., Li, X.C., 2019. Application of nuclear magnetic resonance technology to carbon capture, utilization and storage: a review. J. Rock Mech. Geotech. Eng. 11, 892–908.
Xu, Z., Huang, R., Tang, Z., 2005. Kinetics of silicate mineral dissolution and its implications for landslide studies. Chin. J. Rock Mech. Eng. 24 (9), 1479–1491 (in Chinese).
Ye, Z.N., Liu, X.L., Sun, H., Dong, Q.X., Du, W.S., Long, Q.J., 2022. Variations in permeability and mechanical properties of basaltic rocks induced by carbon mineralization. Sustainability 14 (22), 15195.
Zhang, L., Wen, R., Li, F., Li, C., Sun, Y., Yang, H., 2023. Assessment of CO_2 mineral storage potential in the terrestrial basalts of China. Fuel 348, 128602.
Zhang, R., Zhang, X., Guy, B., Hu, S., de Ligny, D., Moutte, J., 2013. Experimental study of dissolution rates of hedenbergitic clinopyroxene at high temperatures: dissolution in water from 25 °C to 374 °C. Eur. J. Mineral 25 (3), 353–372.
Zhou, Y., Wang, R., Lu, X., 2011. Anorthite dissolution promoted by bacterial adhesion: direct evidence from dialytic experiment. Sci. China Earth Sci. 54 (2), 204–211.
Zhu, W.L., Fusseis, F., Lisabeth, H., Xing, T.G., Xiao, X.H., De Andrade, V., Karato, S., 2016. Experimental evidence of reaction-induced fracturing during olivine carbonation. Geophys. Res. Lett. 43 (18), 9535–9543.

Xiaomin Cao is a doctoral candidate from Institute of Rock and Soil Mechanics, Chinese Academy of Sciences, Wuhan, China. She obtained her BSc degree in Civil Engineering from Sichuan University, China. Her current interest is to understand the hydro-mechanical-chemical coupling mechanism of carbon mineralization in basalt.